Economic Geology, v. 105, pp. 43–68

The Bingham Canyon Porphyry Cu-Mo-Au Deposit. I. Sequence of Intrusions, Vein Formation, and Sulfide Deposition

Patrick B. Redmond[†,*] and Marco T. Einaudi

Department of Geological and Environmental Sciences, Stanford University, Stanford, California 94305 USA

Abstract

The Bingham Canyon porphyry copper-gold-molybdenum deposit is one of the largest and highest-grade porphyry orebodies in the world. This study focused on the northwest side of the deposit where quartz monzonite porphyry (QMP), the first and largest porphyry intrusion, hosts the bulk of the high-grade copper-gold ore (>1.0% Cu, >1.0 ppm Au). The north-northeast–trending, high-grade zone had pre-mining dimensions of 1,500 m strike, >300 m vertical, and 500 m width and contained more than 500 million tonnes (Mt) of ore associated with potassic alteration and abundant quartz veins. The lack of superimposed sericitic alteration yielded ideal exposures in which to study the early, high-temperature stages of ore formation, a style of mineralization that in many porphyry deposits represents the major period of copper introduction.

We mapped multiple porphyry dikes in the sequence: (1) QMP, (2) latite porphyry (LP), (3) biotite porphyry (BP), (4) quartz latite porphyry breccia (QLPbx), and (5) quartz latite porphyry (QLP). Porphyry dikes, faults, and quartz veins are steeply dipping and have two dominant orientations; north-northeast– and northwest-striking. Dikes have a north-northeast strike but they thicken and develop northwest-trending apophyses and host high-grade copper-gold zones at intersections with northwest-faults, indicating that magmatic-hydrothermal fluids were focused by these structural intersections.

Each porphyry intrusion was accompanied by a similar sequence of veins, potassic alteration, and sulfides. Biotite veinlets were followed by fractures with early dark micaceous (EDM) halos of sericite, K-feldspar, biotite, andalusite, and local corundum containing disseminated bornite-chalcopyrite-gold. EDM halos are cut by multiple generations of A-quartz veins representing the main Cu-Au ore-forming event. Postdating all intrusions are quartz-molybdenite veins followed by quartz-sericite-pyrite veins.

Cathodoluminescence (CL) petrography identified distinct A-quartz veinlets consisting of dark-luminescing quartz filling fractures and dissolution vugs in earlier A-quartz veins and adjacent porphyry wall rock. These veinlets contain abundant bornite and chalcopyrite and minor K-feldspar and are closely linked in time to the introduction of the bulk of the copper and gold. Although a similar sequence of veins was repeated on emplacement of all porphyry intrusions, the vein density and intensity of potassic alteration declined with time. The youngest porphyry, QLP, is mostly weakly mineralized and locally unaltered. These observations indicate that magmatic-hydrothermal fluids underwent a similar physiochemical evolution during and immediately following emplacement of each of several porphyry dikes. The relationship between EDM veins and A-quartz veins requires that the flux of magmatic fluid from the magma chamber occurred in an episodic manner as opposed to a continuous discharge.

Vein truncation relationships coupled with abrupt changes in copper-gold grades, sulfide ratios, and potassic alteration intensity at porphyry intrusive contacts indicate that the mass of introduced copper and gold decreased significantly during successive porphyry intrusive-hydrothermal cycles, presumably due to depletion of metals and volatiles in the underlying magma chamber.

Introduction

The genetic link between porphyry copper deposits and magmatic-hydrothermal processes is well established, based on mapping and petrological studies (Gustafson and Hunt, 1975; Dilles and Einaudi, 1992; Proffett, 2003), characteristics of fluid inclusions (Roedder, 1971; Nash, 1976; Eastoe, 1978; Bodnar, 1995; Heinrich el al., 1999; Ulrich et al., 1999, 2002; Audetat et al., 2008), light stable isotopes (Sheppard et al., 1969, 1971; Harris et al., 2005), and analogy with active volcanic fumaroles and geothermal systems (Henley and McNabb, 1978; Hedenquist and Lowenstern, 1994; Einaudi et al., 2003). Formation of porphyry copper deposits requires the escape of magma and hydrothermal fluid from a magma chamber located well below the deposit (Proffett, 2009), and precipitation of sulfides in structurally focused zones as a consequence of cooling, interaction with wall rocks, boiling, and/or mixing with meteoric waters (Gustafson and Hunt, 1975; Brimhall, 1979; Reynolds and Beane, 1985; Hemley and Hunt, 1992; Inan and Einaudi, 2002; Harris et al., 2005; Gruen et al., 2010; Landtwing et al., 2010).

Historically, papers on Bingham have shown copper and gold grade boundaries that encompass all porphyry intrusions, and the timing of sulfide deposition relative to the intrusive sequence and different vein types has not been resolved (James et al., 1961; John, E.C., 1978; Phillips et al., 1998). Of the world's porphyry copper deposits, Bingham ranks seventh based on contained copper metal (28 Mt), second based on contained gold (1,600 t), and fifth based on copper grade (Cooke et al., 2005). Therefore, extending our understanding of

Acronyms Used in this Paper

EDM = early dark micaceous
LP = latite porphyry
QLP = quartz latite porphyry
QLPbx = quartz latite porphyry breccia
QMP = quartz monzonite porphyry

[†] Corresponding author: e-mail patrick.redmond@teck.com

[*] Present address: Teck Ireland Ltd., 5 Wentworth Place, Wicklow, County Wicklow, Ireland.

Submitted: June 16, 2009
Accepted: December 15, 2009

Bingham is important to developing theories regarding the formation of giant, high-grade porphyry deposits.

Our study focuses on the high-grade zone of >1 percent copper and >1 ppm gold along the axis of porphyry intrusions. We examine the link between grades of copper and gold relative to district structure, vein types, and alteration in the context of time lines established by mapping crosscutting relations between multiple porphyry intrusions. Mapping provides compelling evidence that a regional structural grain of extensional origin was the first-order control on dike emplacement, quartz vein attitudes, and ore trends. Each porphyry intrusion was accompanied by a similar sequence, but at declining intensity, of veins, potassic alteration, and copper-gold mineralization. We document the presence of early, high-temperature veins, similar to the early dark micaceous (EDM) veins of Butte, Montana (Meyer, 1965), that represent the first, although minor, introduction of copper and gold at temperatures of 500ºC. We suggest that these veins indicate a magmatic source region at 3.0 km below the present pit bottom at paleodepths of about 5 km.

Methods

We mapped approx. 3,000 m of bench face in the QMP-LP zone (Fig. 1) at a scale of 1:600, with emphasis on intrusive contacts between porphyries, age of veins relative to each other and to porphyries, and changes in vein abundance, sulfide ratios, and alteration style across porphyry contacts. In order to document the grade of individual porphyry dikes and changes in grade across intrusive contacts, we augmented mine blast hole and diamond drill hole assays with assays from 74 representative chip samples (0.5–6 kg in size) from different porphyry intrusions (see App. 1 for assay data and sample location map).

Two thousand meters of diamond drill core was logged at scales of 1:240 and 1:600, using the same approach used for mapping. Approx. 200 sawed samples were examined using a binocular microscope. Seventy-five polished thin sections were studied by standard transmitted and reflected light microscopy and 30 of these were examined using an SEM and CL detector.

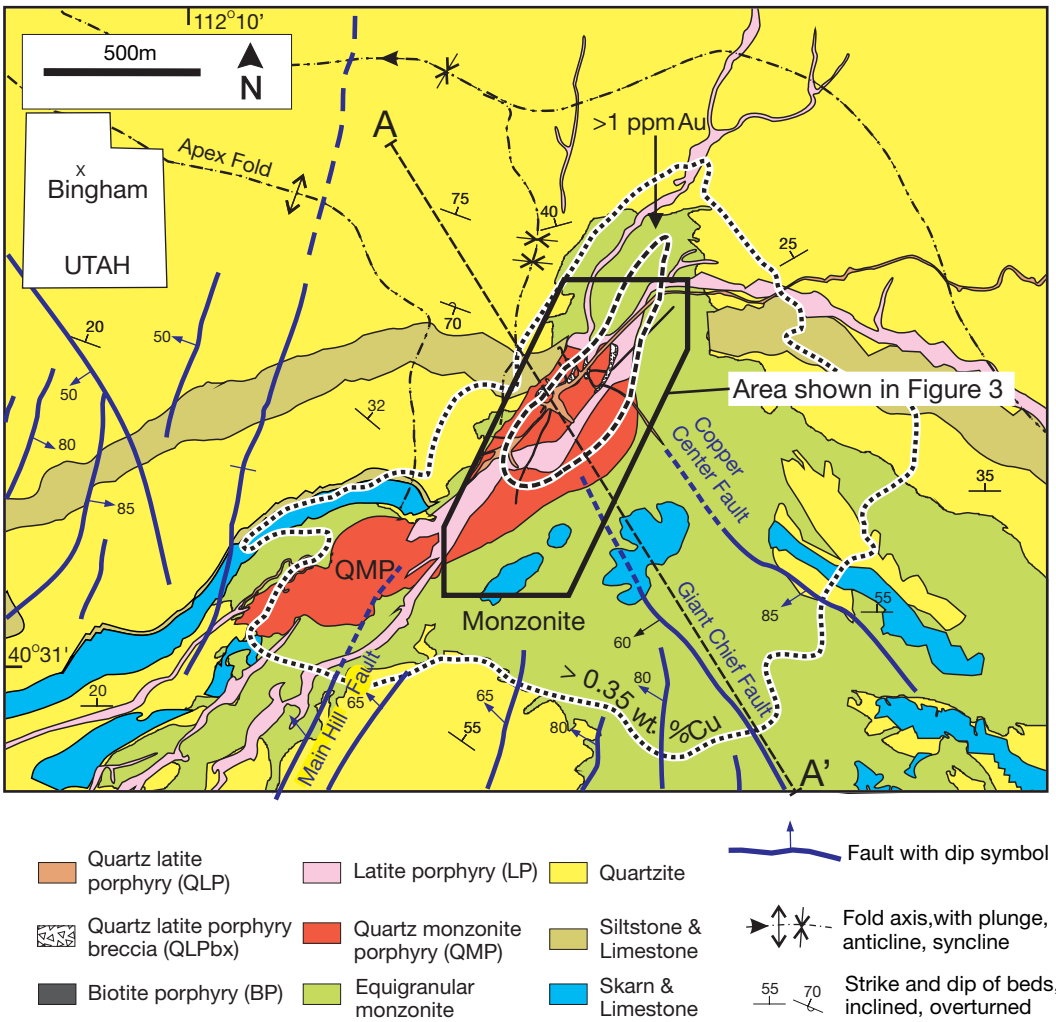

FIG. 1. Composite geologic map of the Bingham porphyry deposit, illustrating the location of faults, morphology of intrusions, and copper and gold grades. Based on unpublished mine geology maps by A.J. Maughan and A.J. Swenson (1990), and Utah Copper geology staff in prior years, 1:600 scale open-pit mapping by Redmond (2002) within the box labeled "QMP-LP zone, Fig. 3"), and Atkinson and Einaudi (1978).

Geologic Setting and Igneous Rocks

The Bingham porphyry deposit, located in the Oquirrh Mountains of Utah, is centered on a late Eocene composite pluton, referred to as the Bingham stock (Butler, 1920), that intruded a thick sequence of quartzite, calcareous quartzite, and limestone of the Pennsylvanian Oquirrh Group (Boutwell, 1905; Welsh and James, 1961; Lanier et al., 1978a; Babcock et al., 1995) (Figs. 1, 2). The Bingham stock is one of a series of ore-related granitoid intrusions emplaced along the east-west–trending Uinta Arch during a period of northwest-southeast–directed extension in the mid-Tertiary (Butler et al., 1920; James et al., 1961; Roberts et al., 1965; Zeitz et al., 1969; Tooker, 1971; Stewart et al., 1977; Constenius, 1996; Vogel et al., 1997; John, 1998; Presnell, 1998). The Oquirrh Mountains lie on the eastern edge of the Basin and Range province and were tilted eastward during extensional faulting during mid-late Cenozoic time. Estimates of the degree of postore tilting range from 10° to 25° (Atkinson and Einaudi, 1978; Lanier et al., 1978a; Melker and Geissman, 1998).

The Bingham stock

The Bingham stock is made up of an equigranular monzonite phase that was intruded by a series of ore-related porphyry dikes. Previous studies have recognized three separate porphyries: quartz monzonite porphyry (QMP), latite porphyry (LP), and quartz latite porphyry (QLP) (Stringham, 1953; Bray, 1969; Moore, 1970; Moore and Czamanske, 1973; Lanier et al., 1978a; Babcock et al., 1995; Phillips et al., 1998), although a minette dike is shown on unpublished mine maps by B.F. Stringham (ca. 1950) and is described by Deino and Keith (1998) and Waite et al. (1998). Analysis of zircon yielded U-Pb isotopic ages for monzonite of 38.55 ± 0.19 Ma (Parry et al., 2001) and $^{40}Ar/^{39}Ar$ isotopic ages of hydrothermal biotite in porphyry dikes yield ages ranging from 37.74 ± 0.11 to 37.07 ± 0.21 Ma (Deino and Keith, 1998; Parry et al., 2001). These data suggest that ore-related hydrothermal alteration, associated with the emplacement of the porphyry dikes, began about 0.75 m.y. after emplacement of the monzonite. Our mapping led to the identification of two previously unrecognized porphyry intrusions: biotite porphyry (BP) and quartz latite porphyry breccia (QLPbx). The complete sequence of porphyries (from oldest to youngest) is (1) QMP, (2) LP, (3) BP, (4) QLPbx, and (5) QLP (Fig. 3, Table 1).

Quartz monzonite porphyry: QMP is the earliest and volumetrically largest porphyry intrusion and contains the highest copper and gold grades in porphyry-hosted ore. It dips 55°–60° NW, has a strike length of approx. 1,500 m and a relatively

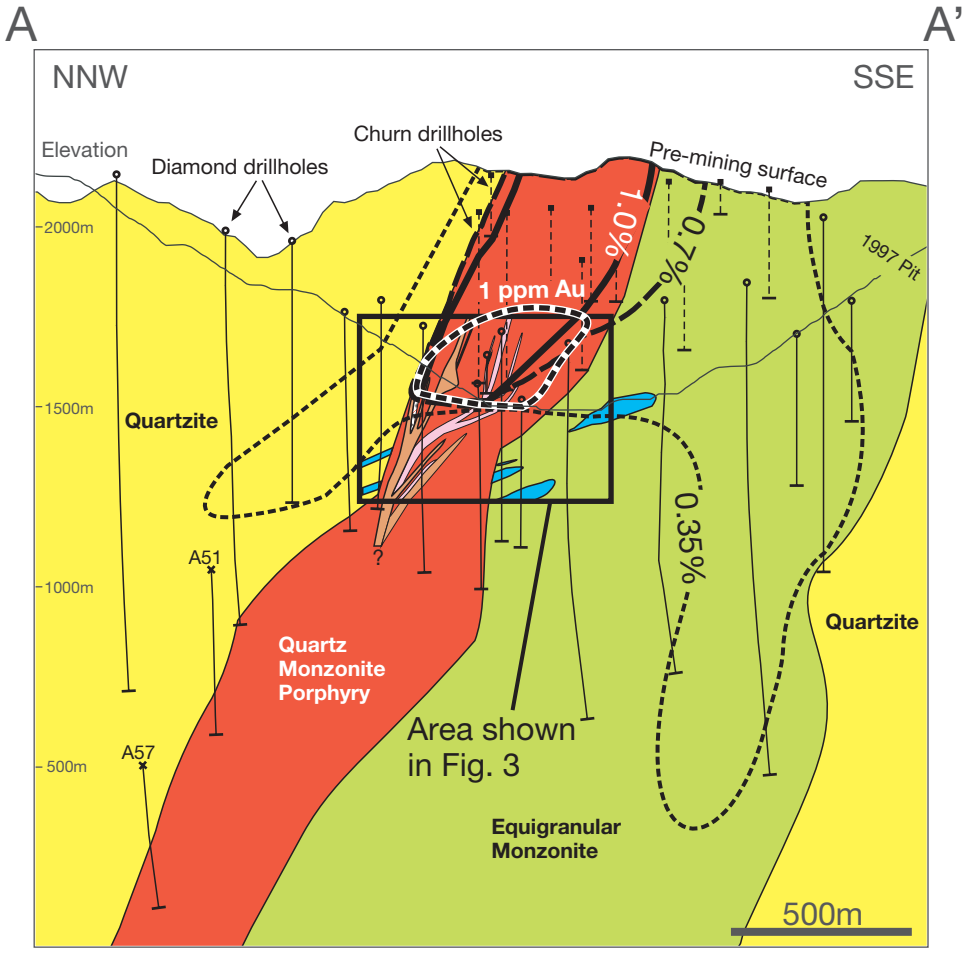

FIG. 2. Geologic cross section A-A' (looking northeast, Fig. 1), showing rock type, copper grade contours and the location of the high-grade gold zone. See Fig. 1 for rock-type legend.

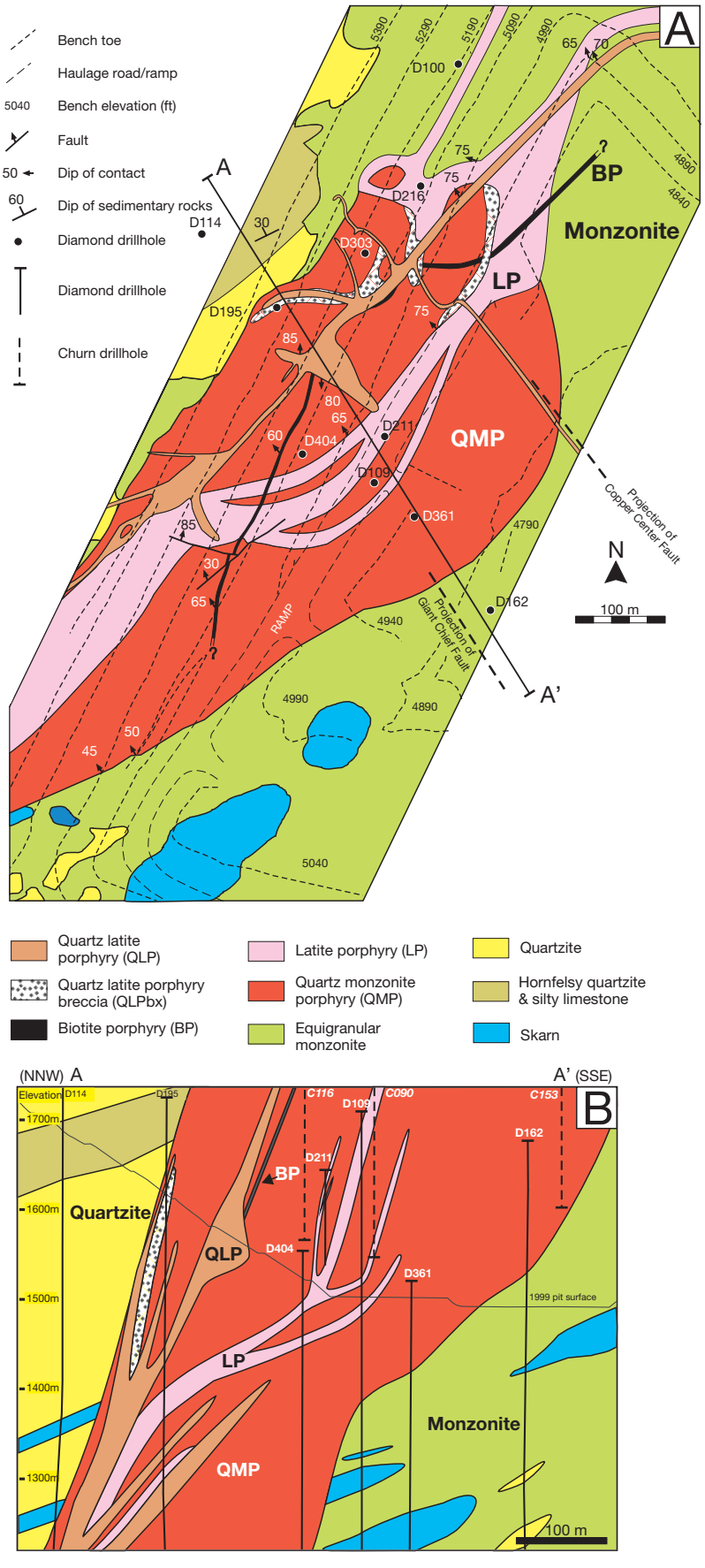

FIG. 3. Detailed geology map (A) and cross section (B) of the QMP-LP zone, showing five porphyry intrusions (see Fig. 1 for location). Copper and gold grades for the same area are shown on Figures 10 and 11.

TABLE 1. Mineralogical Characteristics of Bingham Porphyry Rock Types

	Phenocryst vol % and size range (mm)						
	K-feldspar	Plagioclase	Hornblende	Biotite[1]	Quartz	Pheno vol %	GM vol % and grain size
QMP	6–12% 3–20 mm	25–30% 1–5 mm	12–15% 1–5 mm	2–3% 0.5–1 mm	Rare	50–60	35–50 0.05–0.1 mm
LP	5–10% 2–15 mm	15–20% 1–4 mm	10–12% 0.5–5	2–3% 0.25–2 mm	Rare	50–60	40–50 0.015–0.05 mm
BP	1–5% 1–12 mm	7–15% 0.5–5 mm	2–3% 0.5–5	12–15% 0.25–2 mm	Rare	30–40	60–70 0.02–0.1 mm
QLPbx	1–2% 2–4mm	10–15% 0.5–4 mm	1–2% 0.5–1	2–3% 0.5–1 mm	~1% 2–4mm	20–25	75–80 0.02–0.05 mm
QLP[2]	5–8% 5–45 mm	10–15% 2–8 mm	3–5% 0.5–3	2–4% 0.5–1 mm	3–7% 2–10 mm	30–40	60–70 0.02–0.05 mm

Percentage charts were used to visually estimate mineral abundances in sawn slabs and thin sections; no point counting was carried out
Abbreviations; GM = groundmass, Pheno = phenocryst
[1]Phenocrystic book biotite
[2]Unbiotitized QLP also contains 1.5–2.5% magmatic magnetite and ~1% sphene

constant width of 350 m to depths of 2 km below the premine surface (Figs. 1–3). QMP contains 50 to 60 vol percent phenocrysts of plagioclase, orthoclase, hornblende, biotite, and rare quartz eyes (Table 1). Unaltered groundmass is aplitic (50–100 μm) and composed primarily of subequal amounts of quartz and orthoclase.

Latite porphyry: LP (Bray, 1969; Moore, 1970; Lanier et al., 1978b) occurs as a series of north-northeast–striking dikes and sills that extend for over 3 km along the northwest margin of the Bingham stock (Fig. 1). LP dikes within the QMP-LP zone are 10 to 80 m wide and dip at 60°–75° NW (Fig. 3). LP and QMP are similar in terms of phenocryst and groundmass composition (Table 1). Contacts between the two porphyries are sharp (Fig. 4A), with no chilled margins on LP.

Biotite porphyry: BP cuts both QMP and LP and is in turn truncated by, and occurs as xenoliths within, QLPbx (Fig. 4D). The dike is much darker in color than the other four porphyries owing to the presence of abundant phenocrystic and groundmass biotite (see App. 2 for whole-rock XRF analyses). Pit mapping suggests that BP is continuous for 500 m along its north-northeast strike in the QMP-LP zone, ranges from 2.5 to 4 m wide, and dips 60°–65° NW (Fig. 3). BP contains significantly more biotite phenocrysts (12–15%) than the other four porphyries (2–4%, Table 1). K-feldspar and plagioclase phenocrysts are locally rounded or embayed, likely the result of resorption during emplacement. BP contains small, <5 cm diameter, angular fragments of both QMP and LP. BP is potassically altered and mineralized throughout the study area and locally contains high-grade copper-gold ore and A-quartz veins (e.g., BP sample 5090-1500 assayed 3.5% Cu and 7.1 ppm Au, App. 1). Vein truncation relationships and an abrupt decrease in copper-gold grades at contacts with later porphyries indicate the the high grades in BP are not the result of overprinting by magmatic-hydrothermal fluids from a younger porphyry intrusion.

Quartz latite porphyry breccia: QLPbx cuts QMP, LP, and BP and is in turn cut by QLP that locally displays a <1-cm-wide chilled margin (Fig. 4C). QLPbx is the only porphyry intrusion that contains abundant wall-rock xenoliths. Xenoliths range in size from <1 to 10 cm width, are angular to subrounded, and make up 20 to 50 vol percent of the rock. QLPbx bodies have extremely irregular margins, characterized by abundant 5- to 50-cm-wide dikelets extending several meters into adjacent wall rocks and commonly forming crackle breccia textures. The most extensive exposures of QLPbx were on the 4890 bench, where a 10- to 20-m-wide body extended for 150 m along the north-northeast–striking contact between LP and QMP (Fig. 3). Fragments of QMP and of LP within QLPbx contain multiple generations of truncated A-quartz veins with bornite-chalcopyrite, indicating that QLPbx was emplaced after quartz vein formation and sulfide deposition in LP. In addition, QLPbx contains fragments of BP where it truncates this post-LP dike (Fig. 4D).

QLPbx contains approx. 11 to 17 vol percent phenocrysts of plagioclase and K-feldspar and lesser book biotite, biotitized hornblende, and rare quartz eyes (Table 1). Groundmass is composed of aplitic-textured K-feldspar, quartz, and biotite. Unlike the other four porphyries, the groundmass of QLPbx contains numerous irregular (0.2–1mm) vesicles that make up 2 to 5 vol percent of the groundmass. With the exception of rare grains of fine-grained biotite, these vesicles are unfilled.

Quartz latite porphyry: QLP dikes, first described by Stringham (1953), crop out in the pit for over 3 km (Fig. 1). Wilson (1978) describes an unusual vesicular QLP plug that contained coarse-grained chalcopyrite in quartz-lined vesicles but no vesicular QLP was observed during the current study. Within the mapped area the most continous QLP dike ranges from <10 to 50 m in width and dip 70° to 85° NW. Northwest-striking dikelets and bulbous apophyses of QLP are found where major northwest-striking faults in monzonite project into the north-northeast–striking QMP-LP zone (Fig. 3). Biotitized QLP is medium brown in color and contains about 30 40 vol percent phenocrysts, including 3 to 7 percent quartz eyes (Table 1). Nonbiotitized QLP has a dark green color and

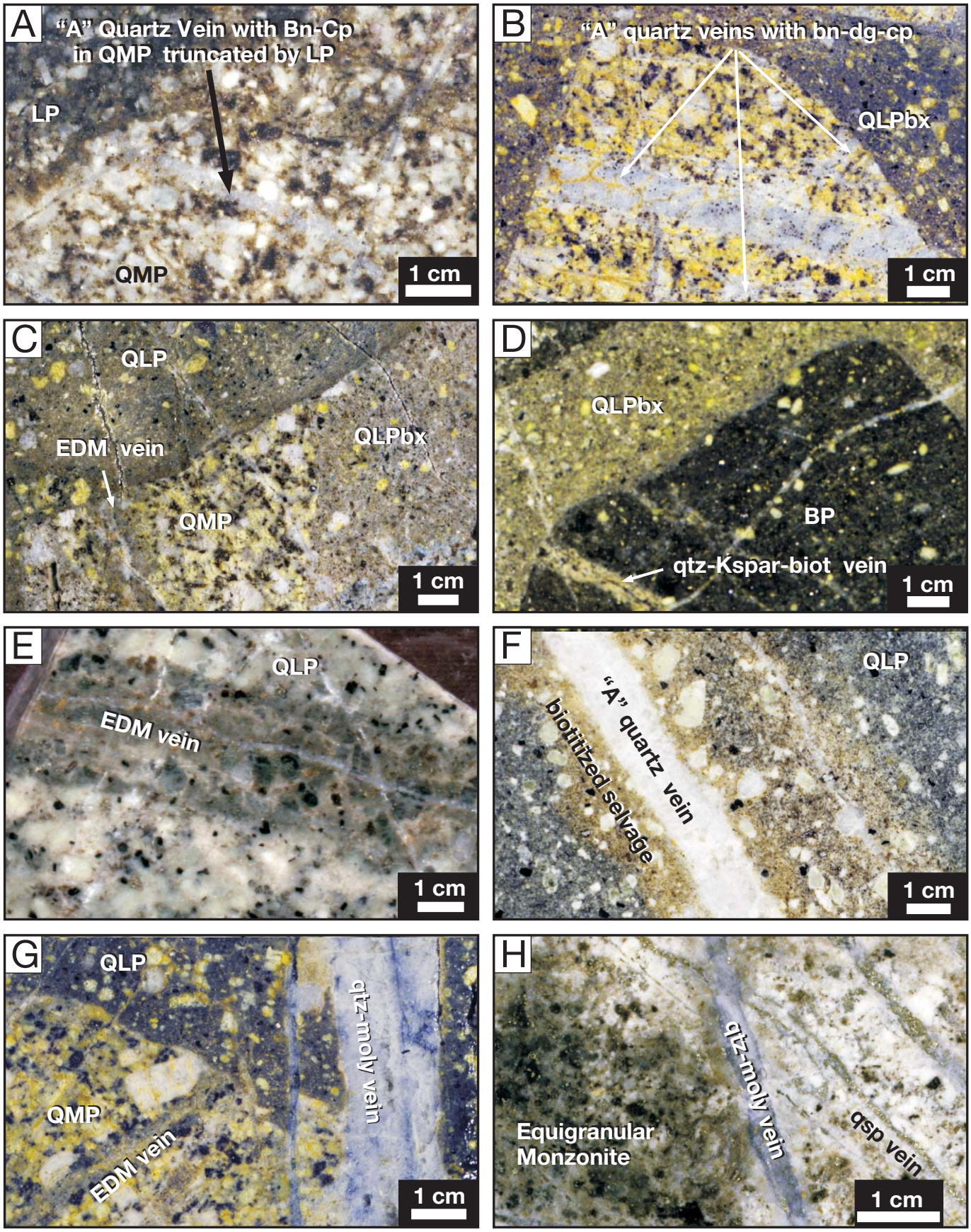

contains unaltered phenocrystic and groundmass amphibole (Fig. 5F). QLP concludes the trend toward increasing abundance of groundmass through the succession of porphyry intrusions (Table 1).

Structural control of porphyry dikes

The dominant faults in the district are steeply dipping, north-northeast–striking faults of probable Mesozoic age reactivated as normal faults during early Basin and Range extension (Farmin, 1933; Tooker, 1971; Atkinson and Einaudi, 1978). These north-northeast faults served as conduits for ore-forming fluids peripheral to the Bingham stock, including vein and replacement Pb-Zn-Ag ores in the US (Rubright and Hart, 1968) and Highland Boy mines (Atkinson and Einaudi, 1978). The most continuous of the north-northeast faults mapped in the open pit, the Main Hill fault zone (Fig. 1), was expressed by pre-mine topography as a deeply incised tributary to Bingham Canyon known as Carr fork (figs. 2, 3 in James, 1978). This fault projects into the main porphyry dike swarm and it is likely that the porphyry dike complex was emplaced along this fault zone.

In addition to the dominant north-northeast faults, a set of northwest-striking faults dipping 50°–85° SW are a secondary control on dike emplacement. The most continuous northwest faults in the open pit are the Giant Chief (Smith, 1975) and Copper Center faults (Fig. 1). Again, pre-mine topography reflects the Giant Chief-Copper Canyon fault zone in the southeast trend of upper Bingham Canyon (figs. 2, 3 in James, 1978).

James et al. (1961) suggested that the zone of intersection of north-northeast and northwest faults was a fundamental control on localizing the Bingham stock at the district scale. At the mine scale, porphyry dikes may have intruded the north-northeast faults. This study demonstrates that locally LP and QLP formed thickened nodes and northwest-striking apophyses at intersections of northwest and north-northeast faults. More importantly, below we present evidence that zones of high quartz vein abundance and high-grade copper-gold ore (defined here as >1% Cu and >1 ppm Au) within the QMP-LP zone are localized at intersections of north-northeast and northwest faults and that the strikes of quartz veins reflect the north-northeast and northwest structural grain of the district.

Veins, Wall-Rock Alteration, and Sulfide Mineralization

Based on our mapping, we have identified a sequence of veins that formed after the intrusion of each porphyry, and, therefore, in a cyclical sequence repeated at least four times (EDM veins were not recorded in BP). A single sequence consists, from early to late (Table 2), of (1) biotite veinlets, (2) EDM veins, and (3) A-quartz veins, all intimately associated with potassic alteration. Postdating all intrusions are (4) quartz-molybdenite veins, and (5) minor, youngest quartz-sericite-pyrite veins.

Biotite veinlets

Wispy biotite veinlets are the earliest vein type at Bingham (Phillips et al., 1998), occurring in low abundance in all five porphyries. Our mapping typically found 5 to 10 veinlets per 10 m of drill core or bench face. Biotite veinlets are typically a few centimeters long, 0.5 to 1.0 mm wide, and are composed of medium-brown biotite with no magnetite. Biotite veinlets contain Cu-Fe sulfides only in cases where they are adjacent to younger veins that contain abundant Cu-Fe sulfides. We interpret this textural relationship to indicate that Cu-Fe sulfides were not deposited contemporaneously with biotite veinlets, but were a later addition.

Early dark micaceous veins

EDM veins, following the terminology of Meyer (1965), are characterized by unfilled fractures with alteration halos in which plagioclase phenocrysts are replaced by andalusite (10–15%), biotite (15–20%), sericite (30–40%), and K-feldspar (25–45%) (Figs. 4, 5). Trace corundum (<1%) is not in contact with rare quartz. EDM halos are 5 to 40 mm wide and are continuous over several meters. Andalusite and biotite are locally replaced by sericite, which is in turn replaced by K-feldspar, a reaction sequence recognized in EDM veins at Butte, Montana (Meyer, 1965; Brimhall, 1977). K-feldspar partially to completely replaces plagioclase phenocrysts in high-grade samples that also contain younger A-quartz veins with K-feldspar halos. This relationship suggests that at least

FIG. 4. Photographs of porphyry contacts and vein relationships. All samples are from open pit exposures unless otherwise noted. See Appendix 1 for sample locations. A. Contact between QMP and LP. Note the A-quartz vein in QMP truncated by LP. Visual estimate of copper grade in QMP is 0.7 percent and in LP is 0.4 percent. Sample no. 4990-1000. B. High-grade xenolith of QMP in QLPbx with multiple truncated A-quartz veins. QMP and QLPbx from this sample were assayed separately. The QMP xenolith sample (sample no. 5190-1910A; sample weight 840 grams) assayed 2.2 percent copper and 5.6 ppm gold. The QLPbx sample (sample no. 5190-1910B; sample weight 1,070 grams) assayed 0.21 percent copper and 3.7 ppm gold. QMP is potassically altered (weakly developed;, see Table 3). Alkali feldspar phenocrysts are replaced by K-feldspar, hornblende is replaced by shreddy hydrothermal biotite and plagioclase phenocrysts are yellow in color due to late illite-smectite alteration. C. Intrusive contact between QLP and QLPbx. Note the xenoliths of QMP with a truncated EDM vein within QLPbx. Yellow color is due to late illite-smectite alteration of plagioclase as in Figure 4B. Sample no. 4990-2150. D. Xenolith of BP with a truncated quartz-K-feldspar-biotite vein enclosed in QLPbx. Visual estimate of copper grade in BP is 2.0 percent and in QLPbx is 0.1 percent. Sulfides consist of bornite-chalcopyrite (with no pyrite) in both porphyries. Late illite-smectite alteration of plagioclase as in Figure 4B. Sample no. 4890-2130. E. EDM vein in QLP. Note that a mineralogically similar EDM vein in QMP is truncated by QLP in image C. Sample no. D126-573 (drill core sample; see Fig. 4 for collar location). F. QLP with fresh hornblende cut by a barren A-quartz vein with a well-developed biotitized halo. Sample no. 4890-2070. G. QMP-QLP intrusive contact. Note the truncated EDM vein in QMP and the quartz-molybdentite vein crossing the contact between the two porphyries. Sample no. 5090-1780. H. Quartz-molybdenum vein cut and offset by quartz-sericite-pyrite veins with sericite halos in equigranular monzonite. Sample no. D411-1593 (drill core sample). Abbreviations: bn = bornite, cp = chalcopyrite, dg = digenite, qtz = quartz, Kspar = K-Feldspar, biot = biotite, qsp = quartz-sericite-pyrite alteration.

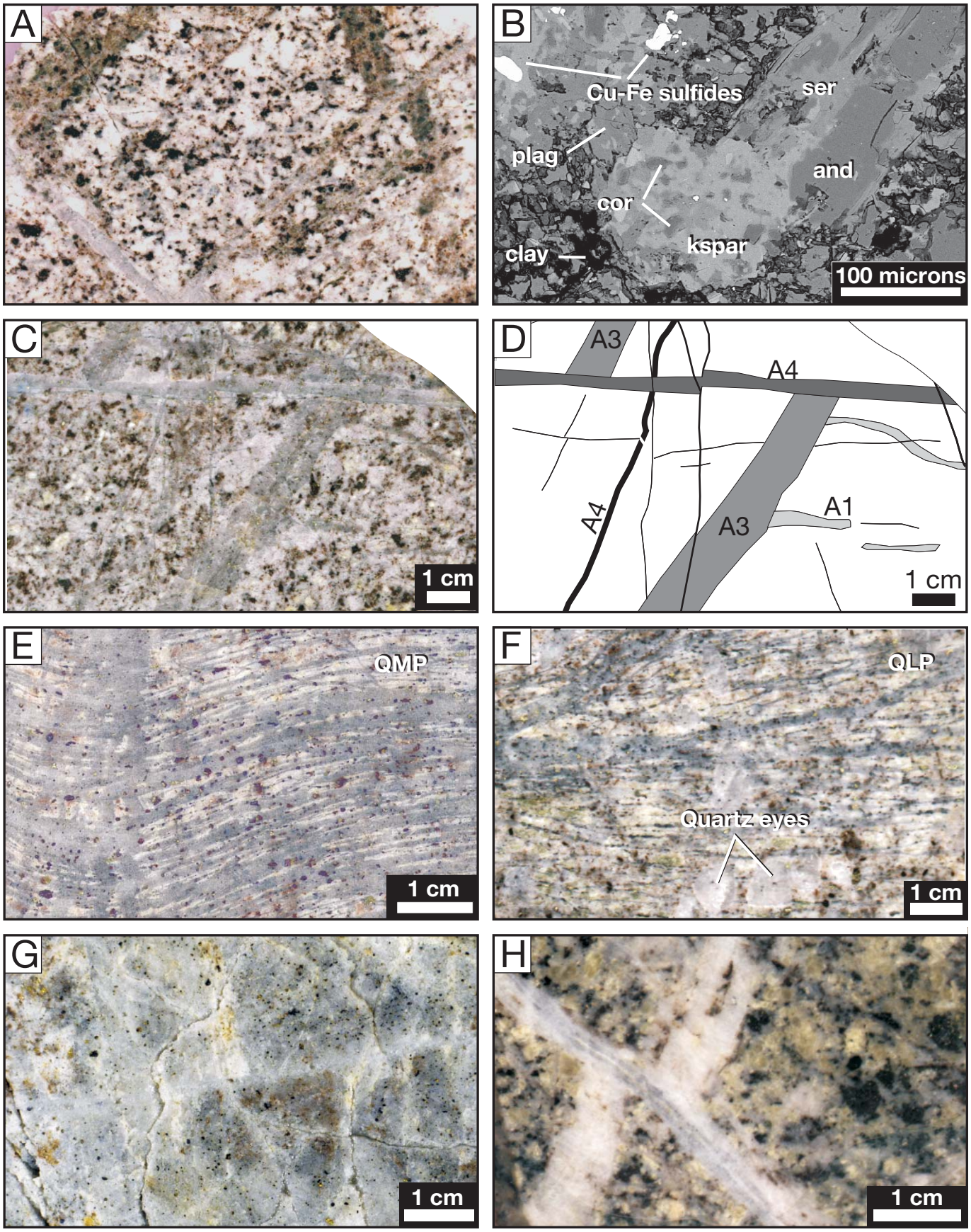

TABLE 2. Major Characteristics of Veins in the QMP-LP Zone (in relative age sequence, oldest at top)

			Vein Fill			Vein Halo		
Vein type	Structure	Length	Width	Gangue, grain size	Sulfides	Width	Gangue	Sulfides
Veins that repeat with each porphyry intrusion								
Biotite veinlets	Wispy seams	Few cm	0.5-1.0 mm	Biot	None, or late bn-cp	None	None	None
EDM veins	Straight-walled	Meters	1-5 mm[1]	Qtz, 0.1-1 mm[1]	bn-dg, cp[1]	5-25 mm	biot, andal, ser, Kspar, ±cor	2-4 vol % dissem. bn-dg, cp
A1 qtz veins	Irregular, discontinuous	10's cm to meters	5-50 mm	Qtz, 0.1-1 mm	bn-dg, cp[2]	1-10 mm	Kspar, qtz, biot	bn-dg, cp[2]
A2 qtz veins	Sheeted sets, commonly sinuous	Meters	0.3-2 mm	qtz, 0.1-1 mm	bn-dg, cp[2]	1-10 mm	Kspar, qtz, biot	bn-dg, cp[2]
A3 qtz veins	Irregular walls, banded	Meters	5-20 mm	qtz, ±Kspar, 0.1-1 mm	bn-dg, cp[2]	1-10 mm	Kspar, qtz, biot	bn-dg, cp[2]
A4 qtz veins	Straight walls	Meters	1-20 mm	qtz, 0.1-1 mm	bn-dg, cp[2]	1-10 mm	Kspar, qtz, biot	bn-dg, cp[2]
A5 qtz-sulfide veinlets	Irreg. veinlets and dissolution vugs	mm to few cm	0.01-0.1 mm	qtz, ±Kspar, 0.01 mm	bn-dg, cp	None	None	None
Veins that postdate all porphyry intrusions								
Qtz-moly	Straight-walled, vuggy	Meters	5-25 mm	qtz, 0.1-10 mm	mo±cp	1-2 mm	Kspar, bio, locally sericite[3]	Trace mo
D-veins	Straight-walled	Meters	5 mm - >1000 mm	qtz, sericite	pyrite	5-100 mm	Sericite	Pyrite

Abbreviations: andal = andalusite, biot = biotite, cor = corundum, cc = chalcocite, cp = chalcopyrite, dg = digenite, Kspar = K-feldspar, mo = molybdenite, qtz = quartz, ser = sericite

[1]Quartz-sulfides in EDM vein centers commonly appear to be the result of later reopening by A-quartz veins

[2]The bulk of the sulfides in A1 to A4 quartz veins were deposited in later A5 quartz-sulfide veinlets that are only visible in thin section with the aid of CL petrography

[3]Usually appears to be related to later quartz-sericite-pyrite stage of alteration

some of this K-feldspar may be related to A-quartz vein formation. EDM halos in the QMP-LP zone contain 1 to 4 percent bornite ± digenite and chalcopyrite, mostly as disseminated grains within biotite and K-feldspar but locally in contact with sericite. One sample of an individual EDM halo in QMP assayed 1.5 percent Cu and 2.6 ppm Au (App. 1, sample no. 5090-1545). We estimate that EDM-hosted sulfides contribute on the order of 1 to 2 percent of the total copper and gold in the high-grade areas of the QMP-LP zone.

EDM vein abundance, highest in QMP, ranges from 1 to 8 veins per 6 m of drill core or bench face (0.25–2 vol %). They were observed in all porphyry intrusions except BP, and vein

FIG. 5. Photographs of veins and wall-rock alteration. All samples are from open pit exposures unless otherwise noted. See Appendix 1 for sample locations. A. EDM veins cut and offset by A-quartz veins in QMP. B. Backscattered electron images showing mineralogy of a replaced plagioclase phenocryst in an EDM halo in LP. Andalusite replaced by K-feldspar. Small corundum grains also occur in contact with K-feldspar. Andalusite is in turn replaced by fine-grained sericite. Small irregular patches of plagioclase are interpreted as hydrothermally altered (now Na-rich) phenocrystic plagioclase and are partly replaced by andalusite, K-feldspar, sericite, and clay minerals. Most of the dark material is fine-grained clay. Clays are interpreted as a late argillic overprint in which plagioclase phenocrysts are replaced by illite-smectite ± kaolinite. Sample no. 4990-1150. C. Sawn rock slab of high-grade QMP from the open pit with multiple generations of A-quartz veins. Sample no. 5090-1550. D. Sketch of image C illustrating cutting and offsetting relations between veins. A discontinuous A1 quartz vein is cut by an A3 quartz vein that is in turn cut and offset by an A4 quartz vein. E. Curved A2 veins in QMP. Sulfides consist of bornite-digenite-chalcopyrite. Sample assayed 2.9 percent copper and 10.04 ppm gold. The porphyry wall rock between the veins is replaced by K-feldspar and quartz and porphyry texture is completely obliterated. Sample no. 5090-1524. F. Curved A2 quartz QLP. Sulfides consist of bornite-chalcopyrite. Sample (715 grams) assayed 1.9 percent copper and 4.4 ppm Au. Note the large quartz eyes and large K-feldspar phenocrysts. Note the textural similarities to veins in QMP in E. Sample no. 5090-1700. G. Sawn rock slab from the open pit with massive blocky quartz and hydrothermal K-feldspar replacing QMP. Example of intense K-feldspar-quartz alteration. Sample assayed 2.1 percent copper and 6.3 ppm gold. Sample no. 5190-880.H. A-quartz veins from deep drill core (drill core sample no. A57-6334) intersection of QMP cut and offset by quartz-molybdenite vein. Abbreviations: and = andalusite, cor = corundum, kspar = K-feldspar, plag = plagioclase, ser = sericite.

truncation relationships at porphyry contacts (Fig. 4G, E) indicate that EDM veins formed during each period of porphyry intrusion. Within each porphyry, EDM veins are cut and offset by multiple generations of A-quartz veins (Fig. 5A). EDM vein abundance is constant within and immediately below the high-grade copper-gold orebody in QMP. Based on logging of drill core in the QMP-LP zone, EDM veins are present from 1,150 m elevation (i.e., 350 m below the base of the high-grade ore) up through the shallowest drill core intersections examined (~1,700 m elev). Therefore, the minimum vertical extent of EDM veins is approx. 550 m.

A-quartz veins

A-quartz veins, as defined by Gustafson and Hunt (1975), are the most abundant vein type in the porphyry orebody (Fig 5A); in QMP they locally exceed 25 vol percent of the rock. Most are 0.5 to 2 cm wide, but some are up to 15 cm wide. Our mapping in the QMP-LP zone shows that the majority of A-veins occur in two dominant sets: north-northeast– and northwest-striking (Figs. 6, 7). A-veins contain digentite, bornite, chalcopyrite, and rare molybdenite. Digenite forms mutual boundaries, lamellae, or grating textures in bornite, but is not in contact with chalcopyrite. Gold grades correlate strongly with copper grades (Fig. 8) and with zones rich in digenite-bornite. Gold occurs predominantly as high-fineness grains 5 to 20 m in diameter (Redmond, 2002).

A-quartz veins occur in all five porphyries, but they are most abundant in QMP, in which four subtypes are recognized megascopically on the basis of structure, texture, and crosscutting relations. These four subtypes are termed A1 to A4 in relative age sequence, with A1 the oldest (Table 2). The sequence A1 to A4, well-defined in QMP, but less so in the younger porphyries, displays a temporal progression from irregular wavy to straight-walled. A1 veins are the most irregular and discontinuous, pinching and swelling along their length (Fig. 5C, D). A2 veins commonly occur in sheeted sets and are sinuous and curved (Fig. 5E, F). A3 veins typically contain thin growth zones of hydrothermal K-feldspar that are subparallel to the vein walls, giving these veins a banded appearance (Fig. 5C, D), similar to the "banding of K-spar" described in some A-quartz veins at El Salvador (Gustafson and Hunt, 1975, p. 882). A4 veins are the most abundant and have relatively straight walls but do not have an obvious center line (Fig. 5C, D). Thin sections of A1 to A4 veins reveal

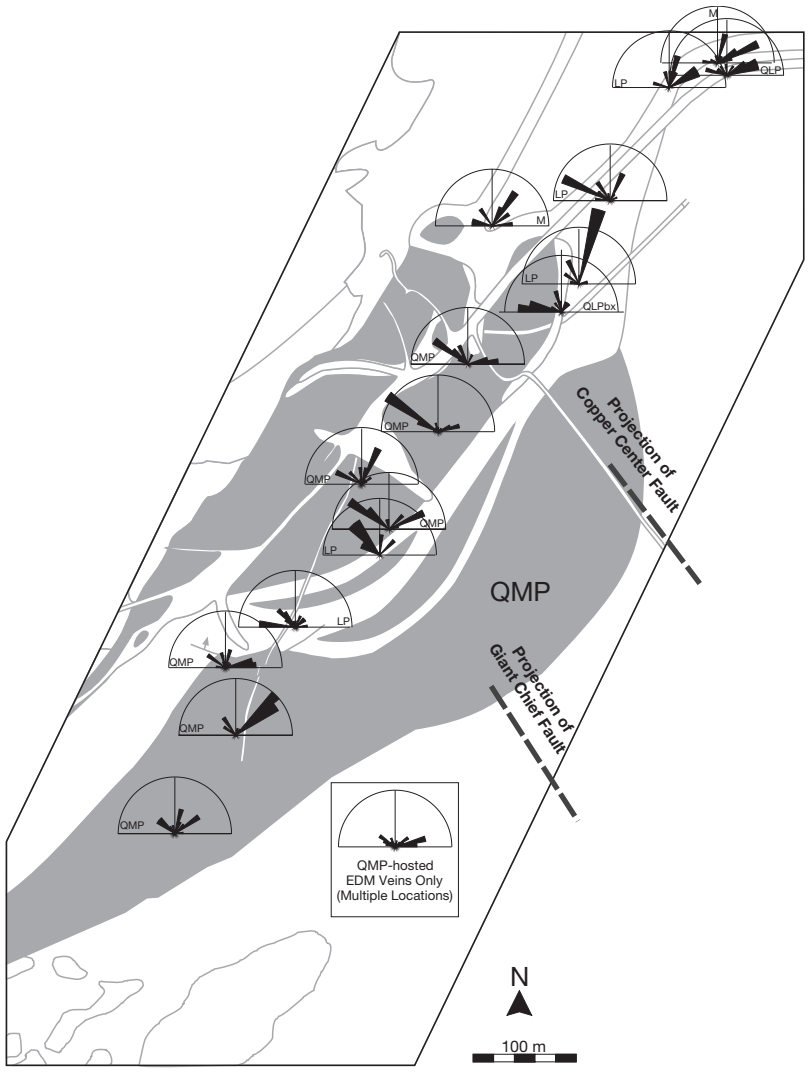

FIG. 6. Maps showing rose diagrams of A-quartz vein orientations for 16 locations within the QMP-LP zone (same area as Fig. 3). Seven of the locations shown are in QMP (shown in dark gray), five in LP, one in QLPbx, one in QLP and two in equigranular monzonite. Each rose diagram represents from 8 to 54 individual vein measurements with an average of 23. Ninety-five percent of the veins have dips between 45° and 85°. EDM vein orientations for multiple locations in QMP are shown on the inset rose diagram.

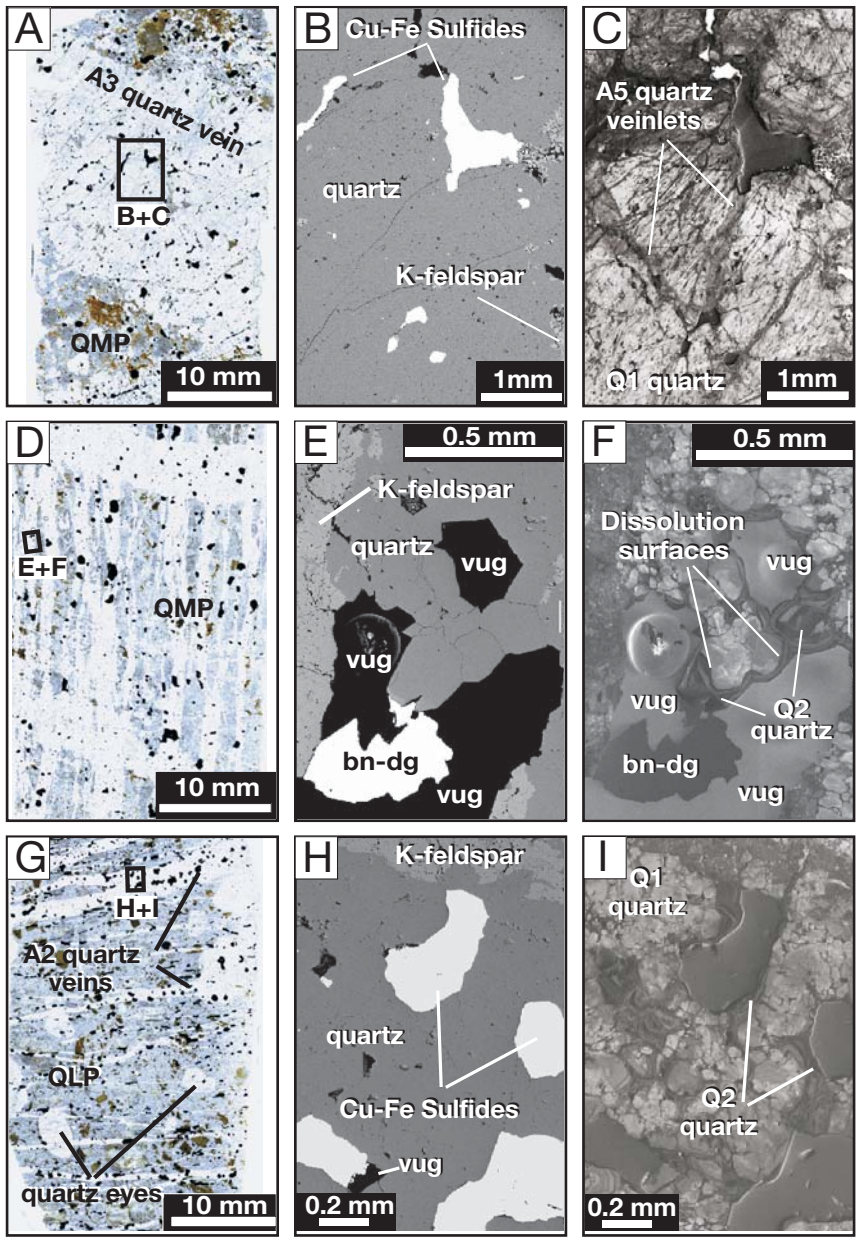

FIG. 7. Textures in high-grade A-quartz veins from QMP and QLP. Note the similarities in vein textures between the two porphyries. Similar textures were also observed in A-quartz veins from LP. See Appendix 2 for sample locations (except drill core samples). A. Transmitted light scan of a thin section showing A3 quartz vein in QMP with abundant copper-iron sulfides (opaque grains). Note the fractures cutting across the vein and the alignment of some sulfide grains along these fractures. Sample no. D404-62.5 (see Fig. 3 for location of drill hole). The location of images B and C is shown by the black box. B. Backscattered electron image of the same field of view as CL image C. Note the empty vugs. C. CL image of the same field of view as B. Abundant A5 veinlets cutting A3 quartz. Note that the orientation of these veinlets is the same as the fractures visible in the scanned thin section shown in image A. The large copper-iron sulfide grain occurs along an irregular vuggy A5 veinlet that contains both A5 quartz and K-feldspar. Note that the epoxy resin in vugs has a bright luminescence. D. Scanned image of a thin section with sheeted, wavy A2 quartz veins with overlapping K-feldspar–quartz halos cutting QMP. Sample no. 5090-1524. Sample assayed 2.9 percent copper and 10.04 ppm gold. Location of images E and F shown by black box. E. BEI of the same field of view as CL image in F showing quartz, K-feldspar, and sulfide grains. Vugs appear black. F. Cl image of the same field of view as image E. Dissolution vug partially filled with dark-luminescing, well-zoned Q2 quartz and a bornite-digenite composite sulfide grain. Growth zones in Q1 quartz are truncated at the contact with Q2 quartz and this contact is interpreted as a dissolution surface. Abbreviations: bn = bornite, dg = digenite. G. Transmitted light scan of a thin section with sheeted A2 quartz veins in QLP. Sample contains abundant copper-iron sulfide grains (opaque grains). Sample no. 5090-1700. Sample was taken from a <1-m-wide zone of high-grade copper-gold mineralization mapped in QLP on bench 5090 (Figs. 9, 10). Note the rounded quartz eyes that characterize QLP. Black box shows the location of images H and I. H. Backscattered electron image of the same field of view as CL image I. Bright grains are copper-iron sulfides. I. Dark-luminescing Q2 quartz filling veinlets and irregular vugs in Q1 quartz. Note the similarities between this sample of QLP and high-grade A-quartz veins in QMP in images C and D.

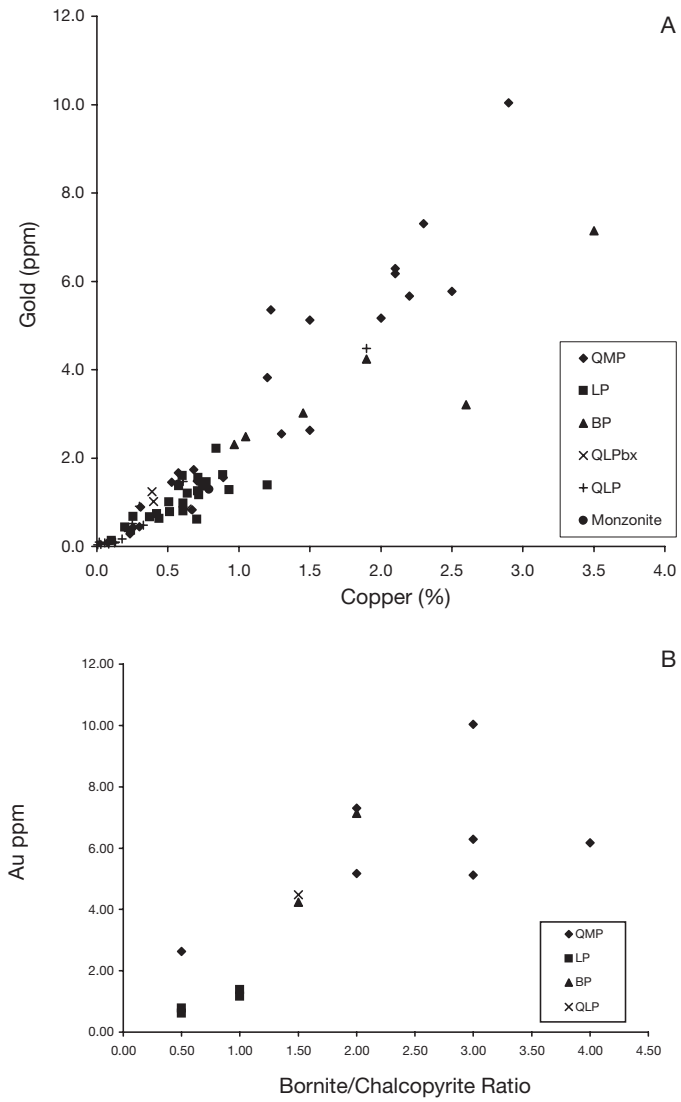

FIG. 8. A. Scatter plot illustrating the strong positive correlation between gold and copper grades for 74 samples of bornite-digenite-chalcopyrite-K-feldspar-biotite-quartz ore (with no pyrite or sericite) from five porphyries and from equigranular monzonite within the QMP-LP zone (see App. 1 for sample locations). B. Scatter plot showing a good correlation between gold grade and bornite/chalcopyrite ratio for 14 samples (of the 74 plotted on A). These small, well-constrained samples were collected in the open pit, and represent four of the five porphyry intrusions.

interlocking anhedral quartz grains, 0.1 to 5 mm in diameter, that are brightly luminescing and weakly zoned in CL, most commonly exhibiting an irregular blotchy texture. We refer to this quartz as Q1 quartz (Fig. 7).

A5 quartz-sulfide veinlets, the dominant ore hosts, are only visible using CL microscopy. They consist of fine-grained (0.01–0.1 mm) dark-luminescing quartz, referred to as Q2 quartz. CL petrography shows that A5 veinlets are typically 0.01 to 0.1 mm wide and range from millimeters to a few centimeters in length. Within the QMP-hosted orebody, all A1 to A4 veins and immediately adjacent porphyry wall rock are cut by numerous A5 veinlets and irregular vugs filled with Q2 quartz, and varying amounts of copper-iron sulfides and dark-luminescing K-feldspar (Fig. 7). Vug margins truncate growth zones in Q1 quartz grains, indicating that vug formation involved quartz dissolution. A5 veinlets and vugs cutting earlier A-veins occur in all five porphyry intrusions (Fig. 7). These are the youngest veinlets in any given intrusion-mineralization event, host the majority of Cu-Fe sulfides, and are therefore the most closely linked in time to the deposition of copper and gold. Fluid inclusions in Q2 quartz show that copper-iron sulfides in A5 veinlets were precipitated at temperatures of 425° to 350°C (Redmond, 2002; Redmond et al., 2004; Landtwing et al., 2005, 2010). Fluid inclusion data also show that lithostatic to hydrostatic decompression occurring during A-quartz vein formation as temperatures declined to around 425°C (Redmond, 2002).

A5 veinlets and vugs also occur within wall rock adjacent to A1 to A4 veins but are less continuous, more irregular, and contain more K-feldspar than A5 veinlets cutting A1 to A4 veins. A5 veinlets commonly contain K-feldspar as a veinlet-filling mineral where they cut alkali feldspar phenocrysts and quartz where they cut quartz grains (Redmond et al., 2004; fig. 1.10). These textures suggest that the vein-forming fluids were close to saturation with quartz and K-feldspar and that wall-rock minerals acted as seed crystals.

Whereas thicker A5 veinlets commonly extend across contacts between A1to A4 veins and wall rock, thinner A5 veinlets in A1 to A4 veins tend to terminate at vein margins. These textures suggest that rheological differences focused A5 fracturing in earlier A1 to A4 quartz veins rather than in wall rock, which resulted in the correlation between higher copper-gold grades and abundance of A1 to A4 veins within (but not below) the QMP orebody.

Intense quartz-K-feldspar alteration

Potassic alteration styles range from weak (biotitization of hornblende with porphyry texture preserved) to strong (granular, vuggy quartz and K-feldspar with porphyry texture obliterated) (Table 3). Within the high-grade QMP-LP zone, the overall intensity of potassic alteration is a function of A-quartz vein abundance.

Zones of intense quartz-K-feldspar alteration are found where A-quartz veins constitute ≥10 vol percent of the rock and alteration halos overlap. Such alteration occurs locally in LP, QLPbx, and QLP, but zones up to 10 m across were observed only in the high-grade copper-gold zone in QMP where grades commonly exceed 2.0 percent copper and 4 ppm gold. In bench faces, these zones are visually striking, with abundant vitreous A-quartz veins and grayish-white wall rock composed of a granular (0.2–1.0 mm) intergrowth of quartz and K-feldspar grains, 1- to 3-mm orange-brown biotite flakes, and gaudy millimeter-sized bornite-digenite and chalcopyrite grains (Fig. 5G). Irregular blocky A1 quartz veins, commonly with brecciated textures, are particularly abundant within these zones. CL petrography shows that entire thin sections (veins and porphyry wall rock) contain a closely spaced network of A5 quartz veinlets and vugs containing abundant copper-iron sulfides. In thin section, biotite flakes are replaced along their margins by quartz, and early biotite veinlets and EDM veins are absent, having presumably been completely replaced by quartz-K-feldspar.

TABLE 3. Types of Potassic Alteration

Intensity	Porphyry groundmass	Plagioclase[1]	K-feldspar	Biotite[2]
Intense	No longer visible; >75% is replaced by 0.1-1.0 mm K-feldspar-quartz; rock may have a porous, vuggy texture	>75% are replaced by 0.1-1.0 mm K-feldspar-quartz	>75% are replaced by 0.1-1.0 mm K-feldspar-quartz; others altered to hydrothermal K-feldspar, commonly pink in color	Biotite greatly reduced in size and abundance; remaining biotite consists of pale brown, thin flakes
Moderate	>25% replaced by 0.1-1.0 mm K-feldspar-quartz along A-quartz vein halos	>25% of plagioclase phenocrysts altered to K-feldspar	Altered to hydrothermal K-feldspar; usually pink in color	Medium brown; slightly reduced in size and abundance
Weak	Dark color; clearly visible with hand lens; <10 % replaced by 0.1-1.0 mm K-feldspar-quartz along A-quartz vein halos.	<10% of plagioclase phenocrysts altered to K-feldspar	Altered to hydrothermal K-feldspar, usually pink in color	Dark brown-black; not reduced in size or abundance

[1]Plagioclase that is not replaced by K-feldspar is commonly altered to Na-rich plagioclase (see App. 3) and the majority of plagioclase phenocrysts have been subjected to varying degrees of late argillic alteration

[2]Includes magmatic book biotite and hydrothermal shreddy biotite (after hornblende)

Quartz-molybdenite veins

The bulk of the molybdenite in the QMP-LP zone occurs in quartz-molybdenite veins that cut and offset A-quartz veins in all five porphyry intrusions. No truncated quartz-molybdenum veins were observed at porphyry contacts or within the numerous xenoliths of QMP, LP, and BP examined in exposures of QLPbx. Thus, these veins postdate all intrusive activity (Fig. 4G). Trace molybdenite occurs locally as isolated grains with copper-iron sulfides in some A-quartz veins and may or may not have been deposited at the same time as quartz-molybdenum veins.

Quartz-molybdenite veins within the open pit, above 1,500 m elevation, are typically 5 to 50 mm wide and are composed of 1 to 10 mm euhedral quartz crystals that are well zoned in CL and have a well-developed vuggy centerline. They commonly contain trace chalcopyrite. In contrast, quartz-molybdenite veins from deep drill holes (A51 and A57 between 100 and 650 m elev) are 1 to 7 mm wide, contain fine-grained quartz, no chalcopyrite, and are commonly wavy and lack a well-developed centerline (Fig. 5H). CL petrography clearly shows that the bulk of the molybdenite in these veins was deposited on the walls of dissolution vugs. The remaining porosity in these vugs is filled by zeolite and/or calcite that are probably younger than the molybdenite (Redmond, 2002, fig. 1.28). Quartz-molybdenite veins at depth cut and offset barren A-quartz veins (Fig. 5H) and also cut thin QLP dikes.

Late hydrolytic alteration

Pyrite veins with quartz-sericite-pyrite halos (D-veins of Gustafson and Hunt, 1975) cut and offset quartz veins and quartz-molybdenum veins (Fig. 4H). D-veins are extremely rare in the QMP-LP zone; we mapped less than 50 D-veins in 3,000 m of bench face. The vein-filling material in these veins was dominated by pyrite (<95%) with local minor chalcopyrite and quartz. Veins were typically 5 mm wide with selvages ranging from 10 to 30 mm wide. However, on strike to the northeast and southwest and at higher elevations, D-veins are more abundant and vein selvages locally overlap to form >10 m wide zones of pervasive sericitic alteration (Lanier et al., 1978b; Babcock et al., 1995; Inan and Einaudi, 2002; Parry et al., 2002).

Mixtures of smectite, illite, ± kaolinite replace plagioclase phenocrysts to varying degrees throughout the Bingham stock but this alteration is most common along north-northeast–striking faults and fractures (Atkinson and Einaudi, 1978; Lanier et al., 1978a). Illite-smectite alteration does not affect K-feldspar and biotite (Fig. 4B–D, G). Within zones of intense K-feldspar-quartz alteration, where plagioclase phenocrysts were totally replaced by K-feldspar in earlier stages, this late argillic alteration is absent because of the lack of plagioclase. Late argillic alteration does not appear to be related to any vein type, is not accompanied by sulfides, and neither alters the local bornite/chalcopyrite ratios nor the grade patterns.

Changes in Mineralization Intensity across Porphyry Contacts

Within the QMP-LP zone, there is generally an abrupt decrease in abundance of A-quartz veins, intensity of potassic alteration, bornite/chalcopyrite ratios and copper-gold grades across contacts from older to younger porphyries (Fig. 9).

Quartz vein abundance

Most A-quartz veins (> 90%) in QMP were truncated by LP (Fig. 4A), indicating that the bulk of ore-forming hydrothermal activity in QMP took place before the intrusion of LP. However, a small percentage (<10%) of Cu-Fe sulfide-bearing A-quartz veins cut the LP-QMP contact, indicating that some copper and gold were also introduced into QMP after emplacement of LP. BP, in turn, truncates most A-quartz veins in LP. All exposures of QLPbx contain abundant fragments of earlier porphyries with truncated A-veins (Fig. 4B). QLP in turn truncates most A-veins in QLPbx. Average quartz vein abundance declines within each of the five successive porphyries in the QMP-LP zone, as follows: QMP 5 to 15 percent (by volume), LP 1 to 5 percent , BP 1 to 5 percent, QLPbx 1 to 2 percent, and QLP <1 percent (Fig. 9A). However, four of the five porphyries (all except BP) locally contain

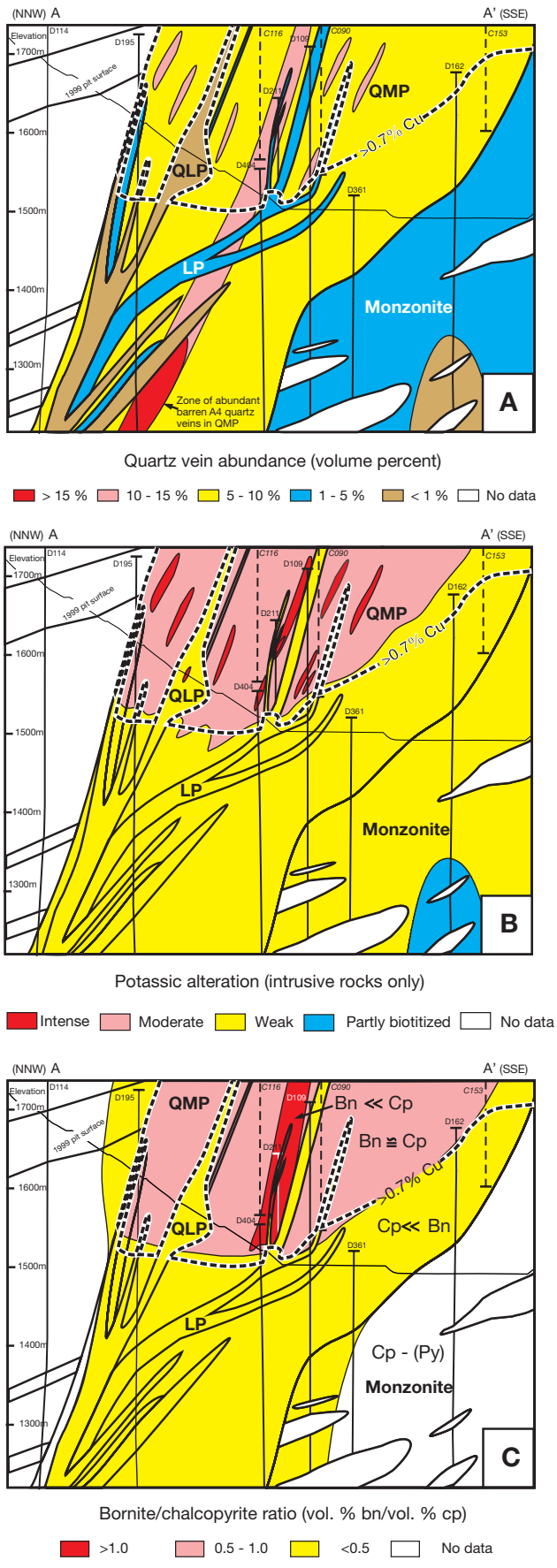

zones 1 to 10 m wide of greater than 25 vol percent quartz veins and associated intense potassic alteration and high-grade copper-gold ore.

Potassic alteration intensity

Potassic alteration intensity (Table 3), as seen in cross section through the QMP-LP zone (Fig. 9B), is highest in QMP. Zones of intense potassic alteration are enclosed within a larger zone of moderate potassic alteration that corresponds closely with the zone of >0.7 percent copper. All younger porphyry dikes have weak to moderate potassic alteration, although both LP and QLP (Fig. 5F) locally contain meter-scale zones of moderate to intense potassic alteration. QLP contains areas, on the order of 10 to 30 m across, that are unaltered except along rare A-quartz veins with selvages in which hornblende phenocrysts are biotitized (Fig. 4F).

Bornite/chalcopyrite ratios

The bornite/chalcopyrite and bornite/digenite ratios of ore in the QMP-LP zone vary considerably both within and between porphyry intrusions (Fig. 9C). The highest bornite/chalcopyrite ratios (1:2–1:1) are found in QMP. In the central portion of this zone (around drill hole D211) bornite/chalcopyrite ratios are greater than 1:1 and locally range up to 10:1. Digenite lamellae in bornite are observed in amounts subequal to bornite only within QMP. An abrupt decrease in bornite/chalcopyrite ratio occurs across the contact from QMP to LP (Fig. 9C); LP is generally chalcopyrite dominant. Exceptions are two narrow LP dikes logged in drill hole D211 and the high-grade (>1% copper) zone in LP around drill hole D216 (Fig. 10) in which bornite is more abundant than chalcopyrite. Chalcopyrite-only and composite chalcopyrite-bornite grains constitute the bulk (>95%) of sulfides in LP; bornite grains with grating-textured digenite are rare. Bornite/chalcopyrite ratios in QLP are generally less than 1:2 (Fig 9C). These observations indicate that bornite/chalcopyrite ratios, and therefore bulk Cu/Fe ratios of sulfides declined with time through the succession of intrusions.

Copper and gold grades

Published grade maps of the Bingham pit (Phillips et al., 1998, their fig. 4) show zones of >1.0, 0.7 to 1.0, and >0.35 percent copper, but grade contours are smoothed across porphyry contacts. In order to document copper and gold grades that reflect observed grade changes across dike contacts, we have interpreted assays from approx. 10-m-spaced blast holes, drill core, and our chip samples (see App. 1 for sample locations), based on mapped relations on pit benches and in drill core (Figs. 10, 11).

FIG. 9. Cross sections (looking northeast) through QMP-LP zone. showing the following: A. abundance of quartz veins, B. intensity of potassic alteration (see Table 3), and C. bornite/chalcopyrite ratios. Section location (A-A') is shown on Figure 3. Rock-type contacts are shown as thin black lines. All drill holes shown on the section were logged at scales of 1:240 or 1:600. Vol percent veins were estimated by measuring average width and average spacing between vein centers for each vein set of a given vein type over intervals of 1 to 10 m in drill core. Potassic alteration was similarly logged and classified in all drill holes shown. Sulphide ratios were estimated visually throughout each drill hole using x20 hand lens and/or binocular microscope.

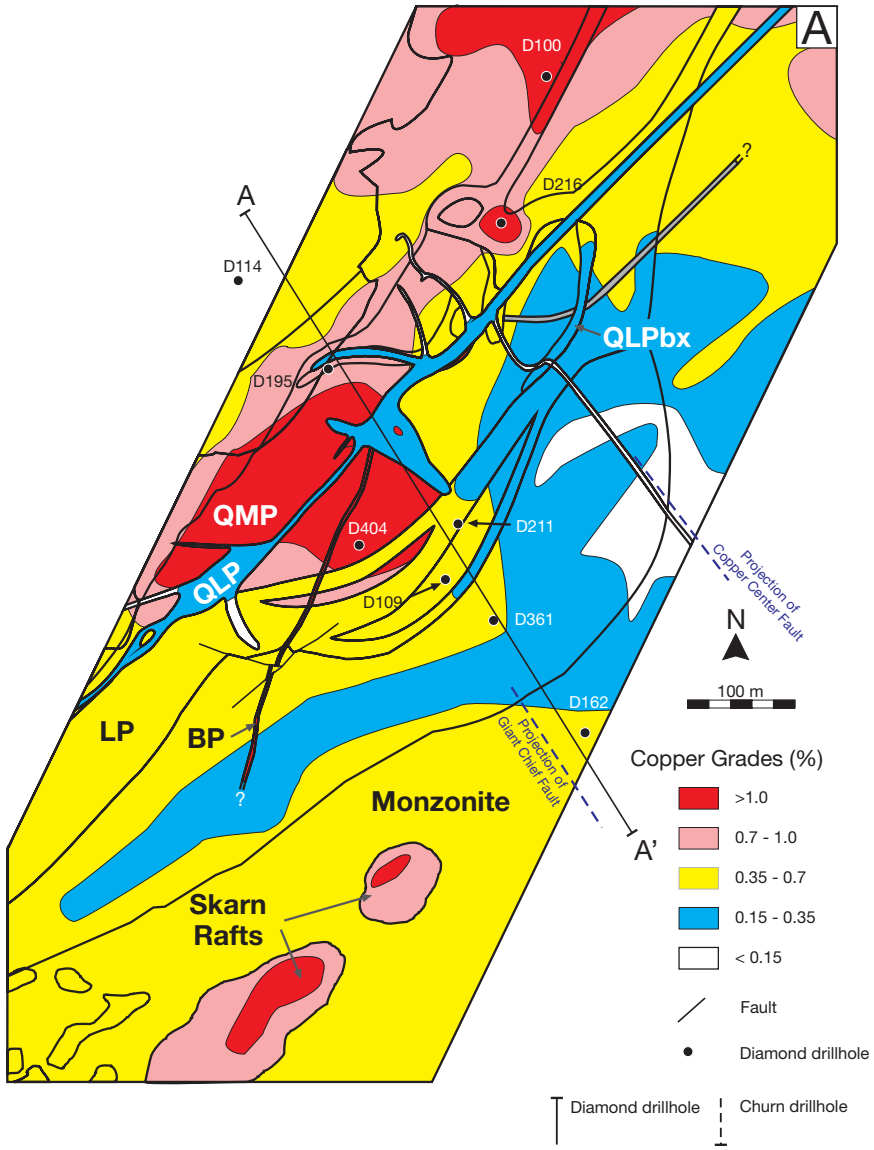

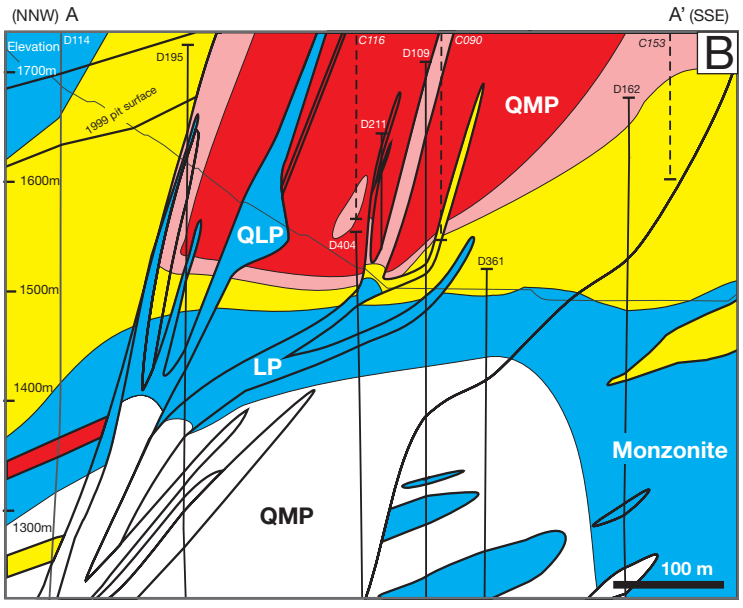

FIG. 10. Map (A) and cross section (B) of QMP-LP zone, illustrating copper grade patterns. A. Area and elevations are the same as on Figure 3. Copper grade data come from four source: (1) assays of blast holes spaced at approx. 10 m, (2) assay data from 45 drill holes within the map area, (3) assay data from 75 bench face chip samples collected in the pit (see App. 3), and (4) grade breaks mapped in the pit and in drill core. B. Grade contours are based on continuous drill core assays (intervals averaging 3.05 m) of all drill holes shown on the section and taken from the mine geology database. Section location (A-A') is shown in A.

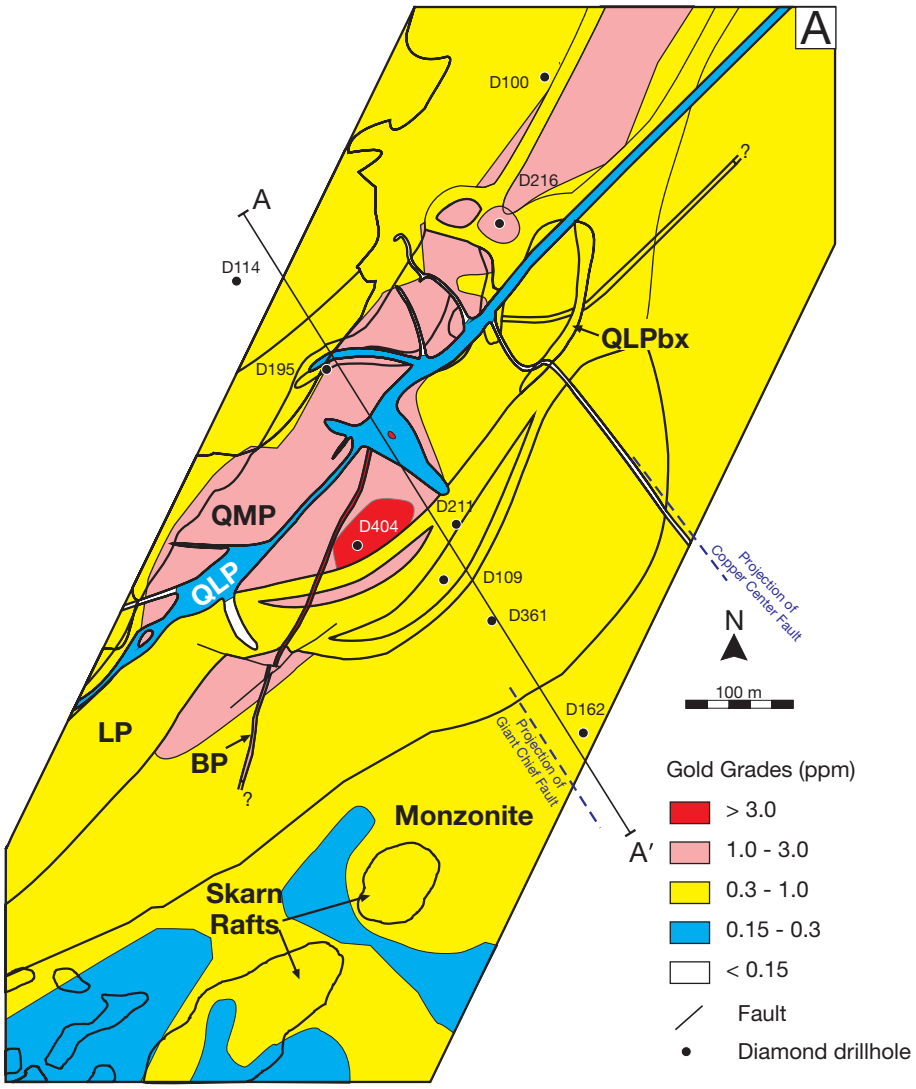

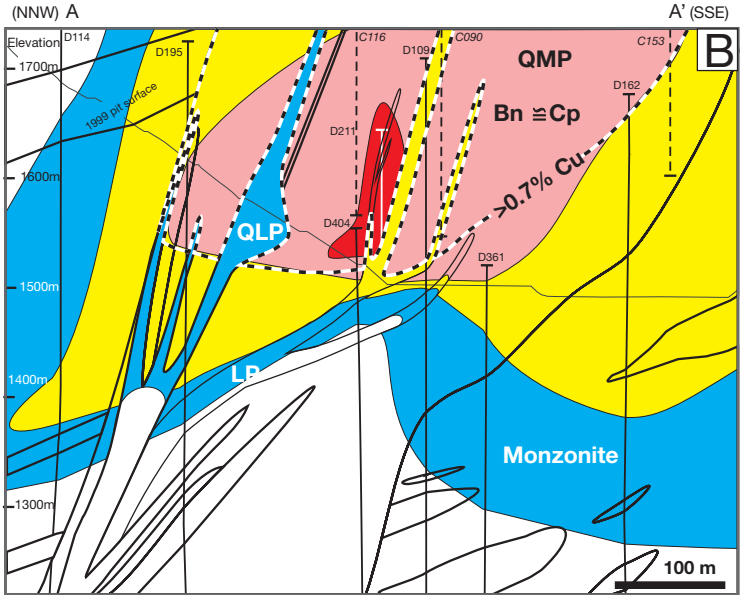

FIG. 11. Map (A) and cross section (B) showing gold grades in QMP-LP zone. Data sources the same as Figure 10. Rock-type contacts are shown as thin black lines.

Within the QMP-LP zone, high-grade copper-gold ore occurs in all five porphyry intrusions and within the equigranular monzonite although the volumes contained in porphyries that postdate QMP are relatively small. The bulk of the high-grade copper-gold ore in the QMP-LP zone is hosted in QMP and monzonite. The zone of >1.0 percent Cu in QMP (at the 1998–1999 pit surface) had dimensions of only 250 × 150 m in plan view (Fig. 10). However, this exposure represented the remaining basal portion of a much larger volume of high-grade copper ore in QMP that may have extended up to the pre-mining surface, a vertical distance of greater than 500 m (Fig. 10). This zone also contains extremely high gold grades, particularly around drill hole D211, which intersected over 100 m of >3 ppm gold. This high-grade ore occurs at the intersection of the north-northeast porphyry trend (Main Hill fault zone) and the projection of the northwest-striking Giant Chief fault (Fig. 1), and the majority of A-quartz veins in this zone mimic these structural trends (Fig. 6). Both copper and gold grades drop off sharply within QMP below approx. 1,500 m elevation, from >1 to <0.35 percent Cu, and from >1 to <0.15 ppm Au over a vertical distance of 35 to 100 m (Figs. 9, 10). This abrupt decline in copper and gold grades at approx. 1,500 m elevation is observed along the entire strike length of QMP and in equigranular monzonite at the southwest and northeast ends of QMP—a strike length of approx. 2 km.

Within the mapped area, LP generally contains lower grades of copper and gold than QMP and grades drop abruptly across QMP-LP contacts (Figs. 10, 11). For example, across a contact from QMP (sample 4990-1380, see App. 1) to LP (sample 4990-1375, see App. 1) on bench 4990 we documented the following abrupt changes: copper grade declined from 2.5 to 0.7 percent, gold grade declined from 5.8 to 0.8 ppm, bornite/chalcopyrite ratio declined from 5:1 to 1:7, A-quartz vein abundance declined from 15 to 5 percent, and intensity of potassic alteration declined from moderate-locally intense to weakly developed. A similar drop in grade from 1.9 to 0.5 percent copper and 5.6 to 1.0 ppm gold occurs across the QMP-LP contact on bench 5190 (see App. 1). We collected representative chip samples from QMP (n = 23) and LP (n = 25), including samples from both sides of intrusive contacts (i.e., 1–5 m apart). The average grade of QMP in these samples was 1.3 pecent Cu and 3.5 ppm Au compared to 0.6 percent Cu and 1.0 ppm Au in adjacent LP. However, LP locally contains high-grade ore: drill hole D126 (Fig. 10) intersected 36 m of LP containing 1.08 percent copper at the intersection of the north-northeast porphyry trend and the northwest-striking Copper Center fault, an intersection also marked by an increase in width of the LP dike. Copper-gold grades in LP drop sharply below 1,500 m elevation, as in QMP.

BP also contains high-grade mineralization with grades locally exceeding those in adjacent QMP and LP. For example, a 2-m-wide BP dike mapped on bench 5090 assayed 1.45 percent copper and 3 ppm gold (sample 5090-710, see App. 1). A representative sample of QMP (sample 5090-713, see App. 1) 3 m northeast of this contact assayed 0.57 percent copper and 1.7 ppm gold.

Abundant mineralized fragments of earlier porphyry dikes commonly increase the overall grade of the QLPbx, but the inherent grade of this intrusion is low. For example, QMP xenoliths carefully sawn out of one QLPbx sample (Fig. 4B) contained 2.2 percent copper and 5.7 ppm gold (sample 5190-1910A, see App. 1) whereas the QLPbx matrix contained only 0.2 percent copper and 0.4 ppm gold (sample 5190-1910B, see App. 1). However, QLPbx locally contains small zones of high-grade copper mineralization—for example: at one location on bench 5090 the igneous matrix of QLPbx was cut by a 2-m-wide zone of abundant 1- to 2-mm-wide, A2 sheeted quartz veinlets with bornite and chalcopyrite and visually estimated grades of >1.5 percent copper. This high-grade zone in QLPbx is also located at the intersection of the north-northeast porphyry trend and the northwest-striking Copper Center fault, suggesting that this structural intersection persisted as an upflow zone for mineralizing fluids through successive porphyry intrusions.

Copper and gold grades in QLP are extremely variable but the dike is generally significantly lower in grade than adjacent QMP or LP (Figs. 10, 11). The main northeast-trending portion of QLP contains 0.15 to 0.35 percent copper and 0.15 to 0.3 ppm gold. However, the dike locally contains meter-scale zones of high-grade mineralization. For example, on bench 5090, a 1- to 3-m-wide zone of abundant A-quartz veins and associated intense potassic alteration assayed 1.90 percent copper and 4.5 ppm gold (Fig. 5F, sample 5090-1700, see App. 1). This high-grade zone is located where the dike thickens and develops a northwest-trending apophysis that is on trend with the projection of the northwest-trending Giant Chief fault. Biotitized QLP at the distal ends of northwest-trending peripheral apophyses contain lower grades of copper (<0.15%) and unbiotitized zones contain even less copper, typically less than 200 ppm.

The above observations regarding copper-gold grades can be summarized as follows (Figs. 10, 11): (1) abrupt grade changes occur at porphyry contacts, (2) there is a general decline through time in the average copper-gold grade of porphyry intrusions, (3) structural intersections between north-northeast–striking porphyry dikes and northwest-striking faults focused hydrothermal fluid flow and mark the location of individual high-grade copper-gold zones in successive porphyry intrusions, and (4) an abrupt decline in copper-gold grades occurs below approx. 1,500 m elevation in all five porphyry intrusions along the entire strike length of the QMP-LP zone. This abrupt decline in grade is limited to the northwest side of the open pit; elsewhere, relatively high grade mineralization persists to greater depth, forming the deep peripheral roots of the +0.35 percent Cu zone (Fig. 2). In these roots, copper grades gradually decrease with depth.

Veins and Alteration below the QMP-LP Zone

We logged three drill holes (D109, D195, and D404) that pass through the base of the high-grade QMP-LP zone (Figs. 3, 10, 11) in order to document the changes in alteration and vein types that accompany the abrupt decline in copper and gold grades below 1,500 m elevation (Figs. 2, 10, 11).

EDM veins are equally abundant within and immediately below the high-grade copper-gold orebody in QMP but were not observed at depths greater than 350 m below the base of high grade (below ~1,150 m elev). EDM veins within this 350-m interval below the QMP-hosted orebody are cut by barren A-quartz veins and account for most of low-grade copper (300–500 ppm) present in QMP at these deeper levels.

Below the base of the high-grade copper-gold orebody of the QMP-LP zone, the abundance of A1 to A4 quartz veins does not change significantly, but the abundance of sulfide-bearing A5 veinlets (observed in CL) and intensity of potassic alteration decline abruptly (Redmond, 2002; figs. 1.17 and 1.18; Fig. 8). Dark luminescing Q2 quartz was observed in some deep samples from below the orebody (down to 1,090 m elev) but generally occurs as overgrowths on anhedral Q1 quartz grains and not in well-developed A5 veinlets.

A number of deep drill holes were completed in the 1970s by The Anaconda Company and two of these drill holes, A51 (1471.2 m deep) and A57 (1942 m deep), intersected QMP between 150 and 600 m elevation (Fig. 2), that is, over 1 km below the QMP-hosted copper-gold orebody. QMP in these deep intersections is pervasively biotitized. Biotite veinlets are the earliest vein type noted, and EDM veins were not observed. Barren A1 toA4 quartz veins are relatively abundant, typically 5 to10 vol percent, and similar to the typical abundance of A1-A4 veins in the QMP Cu-Au orebody above 1,500 m elevation. QMP in these deep holes contains only minor copper: 160 m of 142 ppm copper in hole A57, and 162 m of 155 ppm copper in hole A51. No gold or molybdenum assays were carried out, but given the positive correlation between gold and copper noted above, it is unlikely that gold grades exceed 0.01 ppm. Molybdenum is visually estimated at less than 0.05 percent MoS_2. Trace amounts of chalcopyrite and pyrite were observed in polished thin sections.

Megascopically, the A-quartz veins appear slightly less vitreous than those within the Cu-Au orebody and display a milky white color in hand sample (Fig. 5H). In CL, these veins are composed of anhedral grains of poorly zoned Q1 quartz. K-feldspar alteration halos are not well developed and there are no zones of intense potassic alteration. A5 quartz veinlets are extremely rare and sulfide poor.

Fluid inclusions in these deep quartz veins trapped a single-phase, CO_2-rich, low-salinity magmatic fluid. This fluid ascended and deposited quartz but little sulfide before separating into a brine and vapor approx. 500 m (~1,000 m elev) below the porphyry-hosted orebody at temperatures of around 550° to 500°C (Redmond, 2002; Redmond et al., 2004; Landtwing et al., 2005). Landtwing et al. (2005) showed that the single-phase magmatic fluid transported on the order of 10,000 ppm copper.

CL petrography also shows that quartz dissolution textures are very common in all quartz-vein types in these deep drill holes and dissolution vugs are filled with molybdenite, calcite, and zeolite minerals (Redmond, 2002), but not with Q2 quartz. Dissolution textures are best developed in quartz molybdenite veins. A-quartz veins are cut and offset by quartz-molybdenum veins (Fig. 5H) that cut a number of thin QLP dikes, a relationship similar to that observed in the Cu-Au orebody at higher elevations. Plagioclase is locally altered to illite-smectite, as it is throughout much of the Bingham stock.

Discussion and Conclusions

Through mapping and petrographic study we have defined and characterized a sequence of structurally controlled porphyry intrusions, vein formation, and associated wall-rock alteration leading to Cu-Au-Mo ore formation. The observations presented above lead to conclusions regarding both genetic and exploration aspects of porphyry copper deposits.

Structural controls of dikes, veins, and grade patterns

Ore-related porphyry dikes in the Bingham pit were emplaced along steeply dipping, north-northeast–striking faults of probable extensional origin (Presnell, 1998). This structural control is seen at the district scale where porphyry dikes extend over distances of 6 to 10 km along the same north-northeast trend (e.g., Lanier et al., 1978a).

North-northeast–striking LP and QLP have northwest-striking apophyses and thickened nodes at intersections of north-northeast– and northwest-striking faults (Fig. 3). These intersections also are marked by abundant quartz veins parallel to these two fault sets, intense potassic alteration, and high-grade Cu-Au mineralization in LP and QLP (Figs. 10, 11). We suggest that flow of magmatic-hydrothermal fluids within successive porphyries was focused at these structural intersections.

Vein attitudes in porphyry-type deposits are variable through time, reflecting changing stress regimes imposed both by the magmatic system and regional tectonic stresses (e.g., Tosdal and Richards, 2001). Attitudes of ore-related quartz veins yield information not only on stress fields and fluid flow (Gruen et al., 2010) but also on structural control of metal grades that can be applied in exploration, ore reserve estimation, and mining. At El Salvador, Chile, A-veins are randomly oriented, B-veins commonly have flat dips, and D-veins show a radial pattern centered on the late porphyry (Gustafson and Hunt, 1975). At Bajo de la Alumbrera, Argentina (Proffett, 2003), peripheral dikes define a radial pattern centered on irregular stocks, but a weak north-northwest trend could be either local or regional in origin. D-veins occupy both radial and concentric fractures. At the Endeavor porphyry Cu-Au deposits, Australia (Heithersay and Walshe, 1995; Lickfold et al., 2003), early ore-bearing quartz veins occupy intrusion-centered fractures, whereas veins with hydrolytic alteration suggest that late fluid flow shifted to a far-field stress regime.

In contrast to the above examples, some porphyry deposits have veins and intrusions that reflect mostly far-field stresses. Ore-related A-veins with potassic alteration at the Yerington mine, Nevada (Carten, 1986), occurred mostly in steep, sheeted fractures parallel to the northwest strike of dike swarms and zones of high-grade copper. At structurally deeper levels within the cupola below the Yerington mine orebody and in deep exposures at the nearby Ann-Mason Pass deposit (Dilles and Einaudi, 1992), barren quartz-oligoclase veins are preferentially oriented along the same regional northwest trend. Bingham fits the category of deposits controlled by regional structure, similar to the Yerington mine and Ann-Mason Pass.

One-phase low-salinity fluids and depth to magma source

Fluid inclusions in quartz veins from >500 m below the high-grade orebody in QMP trapped a single-phase, CO_2-rich, low-salinity magmatic fluid (Redmond, 2002; Redmond et al., 2004, Landtwing et al., 2005, 2010). Similar fluid inclusions have rarely been identified in porphyry systems (Roberts, 1973; John, 1989; Rusk et al., 2008) because the trapping of

such fluids takes place at depths not generally exposed and sampled or because such fluid inclusions are present more commonly in deposits with deep source regions. Depth to source region may have a fundamental effect on the characteristics of associated porphyry deposits (Proffett, 2009), including vein types, early alteration styles, sulfide-oxide mineral assemblages, and temporal relations between porphyry intrusions and ore-grade copper. Following Proffett's (2009) criteria, Bingham appears to have characteristics of both deep and shallow source regions, suggesting an intermediate depth to magmatic sources of fluids of about 5 km. If this is the case, and given the paleodepth estimates of 2.0 km for the present pit bottom (Redmond et al., 2004), then the source cupola underlying Bingham was located at 3.0 km below the current base of the pit.

Role of mafic magmas

BP, the third in a sequence of five porphyries mapped during the current study, is relatively mafic in composition (App. 2, Table 1). BP contains 59 to 62 wt percent SiO_2, but it is clearly not the same as the minette dike described by Keith et al. (1998). The abundance of biotite (10–15%) and relatively high chromium content (270–370 ppm), however, suggest an affinity with primitive alkaline magmas. The occurrence of this mineralized mafic dike within the sequence of porphyry intrusions appears to further support the hypothesis that mafic magmas interacted with latitic magmas in the parent magma chamber below Bingham and contributed metals and volatiles to the system (Keith et al., 1998). However, based on our study, if mafic magmas contributed ore-forming components, this contribution was only significant prior to and/or during QMP time as the decline in grade of successive porphyries indicates a depletion of metals and volatiles in the magma chamber through time.

Multiple cycles of porphyry dike emplacement, vein formation, and sulfide deposition

Mapped relationships between veins and porphyry intrusive contacts show that each porphyry emplacement event was followed by a similar sequence of vein formation and potassic alteration leading to copper-iron sulfide and gold deposition (Fig. 12). All five porphyry intrusions contain zones of abundant A-quartz veins, intense potassic alteration, and high-grade copper-gold ore. However, QMP, the first and volumetrically largest porphyry intrusion, hosts the bulk of the high-grade copper-gold ore. Vein-dike relationships indicate that this high-grade ore in QMP is not the product of multiple episodes of overprinting or of continuous flux of ore-bearing hydrothermal fluids, as has been suggested in a number of other porphyry deposits such as the Yerington mine, Nevada (Einaudi et al., unpub. data, 1969–1982; Proffett, 2009), and the Henderson porphyry molybdenum deposit, Colorado (Seedorff and Einaudi, 2004). At Bingham, we argue against significant grade increases from overprinting on the basis of the following: (1) lack of any symmetry in copper grades surrounding dikes that postdate QMP, and (2) absence of a mapped relation between >0.7 percent Cu and the location of late dikes (Fig. 10).

We conclude that the flux of magmatic-hydrothermal fluids and the mass of introduced copper and gold decreased markedly through time as each successive porphyry intrusive-hydrothermal cycle depleted the underlying parent magma chamber of metals and volatiles. Similar patterns of declining grade through successive porphyry intrusions are observed at many but not all (Proffett, 2009) porphyry deposits, including El Salvador, Chile (Gustafson and Hunt, 1975), Bajo de la Alumbrera, Argentina (Proffett, 2003), Los Pelambres, Chile (Atkinson et al., 1996), the Endeavor deposits, Australia (Heithersay and Walshe, 1995; Lickfold et al., 2003), and Ccacalla, Cotabambas, Peru (Perelló et al., 2004). The presence of late, low-grade porphyry intrusions has a bearing on exploration and mining, especially where these late intrusions are large and emplaced in the center of the intrusive complex. At Bingham, late porphyries, being narrow dikes, caused minimal dilution and do not present significant difficulties in mining.

Sequence of vein formation

EDM veins predate A-quartz veins in numerous porphyry deposits, including the type locality, Butte, Montana (Meyer, 1965), Los Pelambres (type 4 veins of Atkinson et al., 1996), El Salvador (EB and C veins of Gustafson and Quiroga, 1995), and Ann-Mason Pass, Nevada (Proffett, 2009). Although EDM halos at Bingham do not contribute significantly to copper grades, in other deposits these veins represent a major early mineralization style. For example, at Butte, Montanna (Brimhall, 1973, 1977), and in the Chuquicamata district, Chile (Proffett, 2009), EDM halos constitute the higher grade parts of the potassic-related ores.

A-quartz veins in QMP display a progression from irregular wavy to straight-walled with time. This pattern is similar to the changes in quartz vein characteristics described at other porphyry deposits (e.g., Gustafson and Hunt, 1975) and is consistent with the transition from plastic to brittle conditions that occurs as rocks cool (Fournier, 1991, 1999). A-quartz veins from the entire 1,500 m vertical interval examined have K-feldspar halos and are similarly abundant within and below the QMP copper-gold orebody. In contrast to early A-quartz veins, A5 veinlets are far less abundant below the orebody, coincident with a reduction in copper-gold grades, potassic alteration intensity, and bornite/chalcopyrite ratios.

Quartz-molybdenite veins constitute the bulk of the molybdenum ore at Bingham, postdate the emplacement of the last porphyry (QLP) and are in turn cut and offset by late quartz-sericite-pyrite veins. A relatively late age for molybdenum mineralization is supported by the Re-Os dating of Chesley and Ruiz (1998). The late timing of molydenum deposition is further supported by the lack of correlation between molybdenum and copper grades in the orebody.

Space-time model of orebody formation

The temporal sequence of veins, wall-rock alteration, and sulfides detailed above, combined with P-T data from fluid inclusions studies (Redmond, 2002; Redmond et al., 2004; Landtwing et al., 2005, 2010) allow us to illustrate the space-time-temperature evolution veins and ore deposition in the QMP-LP zone (Fig. 12).

Bornite-chalcopyrite-bearing EDM halos represent the earliest sulfide-depositional event at Bingham. Similar veins at Butte, Montana, formed between 650° and 550°C during transient fluctuations between lithostatic and hydrostatic

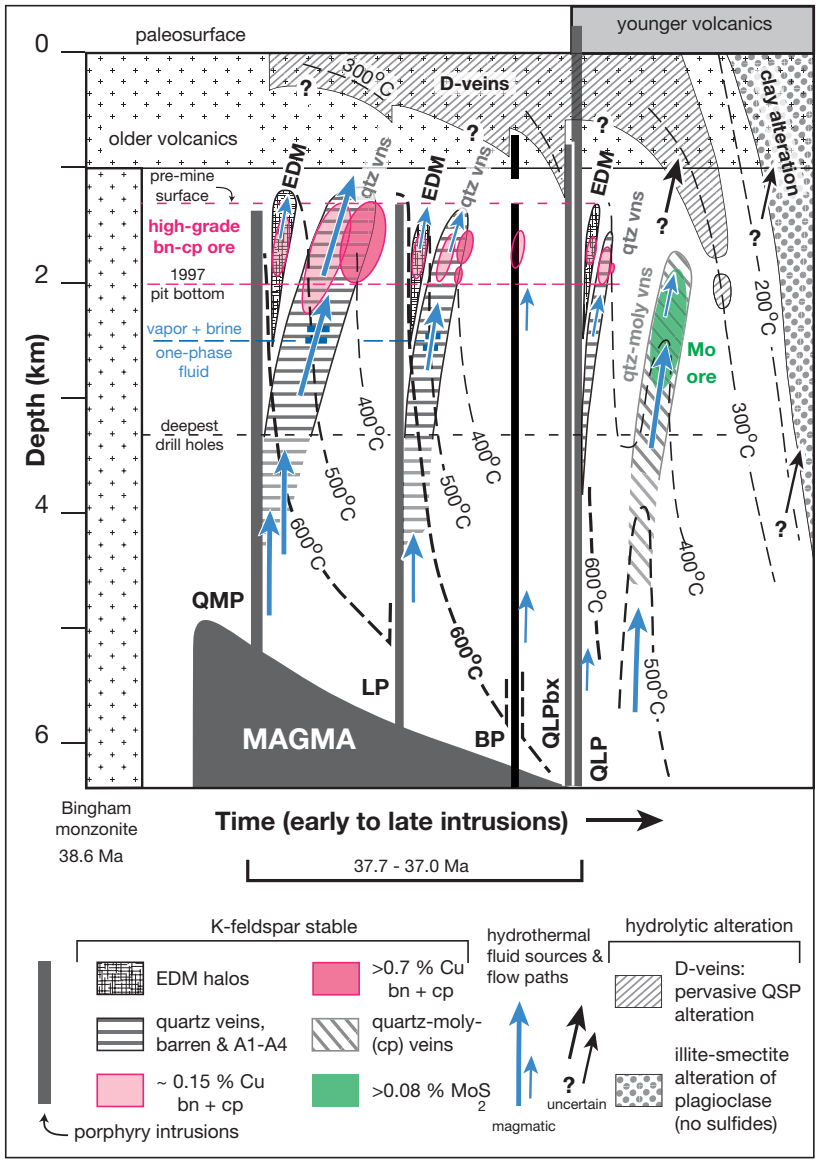

FIG. 12. Time-space-temperature diagram showing evolution of vein types, alteration, and high-grade copper and molybdenum ore based on time lines provided by individual porphyry intrusions. The depth axis is located in center of the QMP-LP zone and relationships shown are based on mapping and core-logging within the depth window of 1.8 to 3.3 km paleodepths. Temperature contours (dashed black lines) and upper boundary of one-phase fluids (blue bars) are based on fluid inclusion studies of Redmond (2002) and Redmond et al. (2004). Time-space distribution of sericitic alteration at paleodepths of <1.5 km is speculative, and this region may have contained silicic and advanced argillic alteration. Abbreviations: bn = bornite, cp = chalcopyrite, moly = molybdenite, QSP = quartz-sericite-pyrite alteration.

pressure at 6 km depth (Roberts, 1973, 1975; Brimhall, 1977; Rusk, 2003; Rusk et al., 2008). Although we conducted no fluid inclusion studies on EDM veins, temperatures of ~550°–500°C are required by the K-feldspar-andalusite-muscovite assemblage at near-lithostatic pressure at the 2 km paleodepth estimated for Bingham (Hemley and Hunt, 1992). EDM halos provide the strongest evidence in porphyry copper deposits for copper deposition at temperatures >500°C. Furthermore, during each period of EDM formation, no A-quartz veins formed (Fig. 12). Therefore, A-quartz veins and major sulfide deposition represent episodic pulses of hydrothermal fluid following each intrusion, rather than representing a continuous flux of hydrothermal fluids, at declining intensity, throughout the period of multiple porphyry intrusions.

Redmond et al. (2004) showed that, following the formation of EDM veins, an ascending, single-phase magmatic fluid formed barren quartz veins at depth prior to phase separation (Fig. 12). Phase separation to coexisting brine and vapor took place approx. 500 m below the base of the high-grade orebody of the QMP-LP zone at 550° to 500°C and ~625 bars pressure (Redmond et al., 2004; Landtwing et al., 2005, 2010). Brine and vapor continued to ascend and cool, due to expansion and heat loss to the wall rocks, forming A1-A4 quartz veins and associated potassic alteration.

Fluid inclusion data indicate that lithostatic to hydrostatic decompression occurred during A-quartz vein formation as temperatures declined to about 425°C (Redmond, 2002). The inferred temperature range is in good agreement with rock mechanics data and observations from active geothermal systems (Fournier, 1991, 1999). The numerous unconformities between CL growth zones in A1 to A4 quartz (Fig. 7) indicate that multiple cycles of quartz precipitation-dissolution-precipitation occurred as a result of pressure fluctuations or cooling in the P-T region of retrograde quartz solubility (Fournier, 1999). Depressurization from lithostatic to hydrostatic pressure conditions causes the muscovite-K-feldspar phase boundary to move toward lower ($m_{KCl + K^+}/m_{HCl + H^+}$) values at any given temperature (Hemley and Hunt, 1992) and would allow hydrothermal fluids to cool even further while remaining in the K-feldspar stability field.

Formation of A5 quartz veins and associated Cu-Au mineralization occured within the K-feldspar stability field as temperatures declined from 425° to 350°C at hydrostatic pressure (Redmond, 2002; Redmond et al., 2004; Landtwing et al., 2005, 2010). We interpret this thermal decline to be the driving force for Cu-Fe sulfide deposition, given the lack of evidence of mixing of hydrothermal fluids with low-salinity waters, the lack of correspondence of the ore zone with the initiation of phase separation, and no change in wall-rock alteration style. This conclusion is strongly supported by laser ablation ICP-MS analyses which show that copper concentrations in fluid inclusions in A5 veinlets drop by two orders of magnitude, within a narrow pressure-temperature interval between 210 and 140 bar and 425° to 350°C (Landtwing et al., 2005). The sharp base to the QMP-LP zone orebody at ~1,500 m elevation (500 m above the zone of phase separation) may represent the location of the 425°C isotherm at the time of ore formation in the QMP-LP zone.

This study provides new evidence and new lines of inquiry regarding the formation of Bingham, and, by analogy, other giant porphyry copper deposits. The inception of extensional faulting may have triggered the emplacement of porphyry magma, but the fact that extension was minor ensured that these magmas and accompanying volatiles did not vent. Structural intersections may have been particularly effective in localizing zones of high-grade copper-gold ore. Intramineral mafic dikes suggest an open-system magma chamber at depth that was replenished through time with ore-forming components, although this may not have been a key factor in generating the large Bingham deposit, given that the bulk of the ore was introduced with the first porphyry intrusion. Finally, EDM halos, a vein type not generally recognized in porphyry deposits, represent a process, at present poorly understood, that led to early, high-temperature deposition of Cu and Au. These early halos formed a low-grade protore that may have subsequently contributed copper and gold during formation of younger A-quartz veins which host the bulk of the copper-gold ore.

Acknowledgments

We thank Geoff Ballantyne, who helped to get this project started and secured funding from Kennecott and access to the mine. We are indebted to Ed Harrison, Tracy Smith, Kim Schroeder, and Ken Krahulec for their help during Redmond's two field seasons at Bingham Canyon. Jim Reynolds provided invaluable assistance with the fluid inclusion portion of this study. This project benefited greatly from collaboration with Chris Heinrich and Marianne Landtwing from ETH. Collaboration with Adrienne Larocque from the University of Manitoba aided our understanding of gold mineralization in the orebody. Jeff Keith from Brigham Young University carried out XRF analyses of samples of BP. MTE thanks John Hunt, Julian Hemley, John Proffett, John Dilles, and Eric Seedorff for many useful discussions on porphyries over the years. The majority of the funding for this research was provided by the Lokey Fund, Department of Geological and Environmental Sciences at Stanford University. Additional funding was provided by the Stanford Shell and McGee Funds and by two Hugh E. McKinstry grants from the SEG Foundation. At Stanford, help and support with Redmond's research was provided by Esra Inan, Denis Bird, Gail Mahood, Bob Jones, Kurt Friehauf, Guillermo Pareja, and John Muntean. Finnian O'Connor helped with final drafting of the figures. Finally, we would like to thank *Economic Geology* referees Steve Kesler, Anthony Harris, and David Cooke for their helpful reviews.

REFERENCES

Atkinson, W.W., Jr., and Einaudi, M.T., 1978, Skarn formation and mineralization in the contact aureole at Carr Fork, Bingham, Utah: Economic Geology, v. 73, p. 1326–1365.

Atkinson, W.W., Jr., Souviron, A., Vehrs, T.I., and Faunes G.,A., 1996, Geology and mineral zoning of the Los Pelambres porphyry copper deposit, Chile: Society of Economic Geologists Special Publications, v. 5, p. 131–156.

Audétat, A., Pettke, T., Heinrich, C.H., Bodnar, R.J., 2008, The composition of magmatic-hydrothermal fluids in barren and mineralized intrusions: Economic Geology, v. 103, p. 877–908.

Babcock, R.C., Jr., Ballantyne, G.H., Phillips, C.H., and Bolm, J.G., 1995, Summary of the geology of the Bingham district, Utah: Arizona Geological Society Digest, v. 20, p. 316–335.

Bodnar, R.J., 1995, Fluid-inclusion evidence for a magmatic source for metals in porphyry copper deposits, *in* Thompson, J.F.H., ed., Magmas, fluids and ore deposits: Mineralogical Association of Canada Short Course Series, v. 23, p. 139–152.

Boutwell, J.M., 1905, Economic geology of the Bingham mining district, Utah: U.S. Geological Survey Professional Paper 38, 413 p.

Bray, R.E., 1969, Igneous rocks and hydrothermal alteration at Bingham, Utah: Economic Geology, v. 64, p. 34–49.

Brimhall, G.H., 1973, Mineralogy, texture and chemistry of early wall rock alteration in the deep undergound mines and Continental area, Butte, Montana: *in* Miller, R. N., ed., Guide Book to Butte Field Meeting, Montana Bureau of Mines and Geology publication O1, p. H1–H4.

——1977, Early fracture-controlled disseminated mineralization at Butte, Montana: Economic Geology, v. 72, p. 37–59.

——1979, Lithologic determination of mass transfer mechanisms of multistage porphyry copper mineralization at Butte, Montana: Vein formation by hypogene leaching and enrichment of potassium silicate protore: Economic Geology, v. 74, p. 556–589.

Butler, B.S. et al., 1920, The ore deposits of Utah: U.S. Geological Survey Professional Paper 111, 672 p.

Carten, R.B., 1986, Sodium-calcium metasomatism: Chemical, temporal, and spatial relationships at the Yerington, Nevada, porphyry copper deposit:Economic Geology, v. 81, p. 1495–1519.

Chesley, J.T., and Ruiz, J., 1998, Preliminary Re-Os dating on molybdenite mineralization from the Bingham Canyon porphyry copper deposit, Utah: Society of Economic Geologists, Guidebook Series, v. 29, p. 165–169.

Clode, C., Proffett, J., Mitchell, P., and Munajat, I., 1999, Relationships of intrusion, wall-rock alteration and mineralisation in the Batu Hijau copper-gold porphyry deposit: Australasian Institute of Mining and Metallurgy, Publication Series, v. 4-99, p. 485–498.

Constenius, K., 1996, Late Paleogene extensional collapse of the Cordilleran foreland and thrust belt: Geological Society of America Bulletin, v. 108, p. 20–39.

Cooke, D.R., Hollings, P., and Walshe, J.L., 2005, Giant porphyry copper deposits: Characteristics, distribution, and tectonic controls: Economic Geology, v. 100, p. 801–818.

Deino, A., and Keith, J.D., 1998, Ages of volcanic and intrusive rocks in the Bingham mining district, Utah: Geology and ore deposits of the Oquirrh and Wasatch Mountains, Utah, 1998, p. 91–100.

Dilles, J.H., and Einaudi, M.T., 1992, Wall-rock alteration and hydrothermal flow paths about the Ann Mason porphyry copper deposit, Nevada; a 6-km vertical reconstruction: Economic Geology, v. 87, p. 1963–2001.

Eastoe, C.J., 1978, A fluid inclusion study of the Panguna porphyry copper deposit, Bougainville, Papua New Guinea: Economic Geology, v. 73, p. 721–748.

Einaudi, M.T., Hedenquist, J., and Inan, E. (2003) Sulfidation state of fluids in active and extinct hydrothermal systems: Transitions from porphyry to epithermal environments: Society of Economic Geologists Special Publication, v. 10, p. 285–313.

Farmin, R., 1933, Influence of Basin-Range faulting in mines at Bingham, Utah: Economic Geology, v. 28, p. 601–606.

Fournier, R.O., 1991, The transition from hydrostatic to greater than hydrostatic fluid pressure in presently active continental hydrothermal systems in crystalline rock: Geophysical Research Letters, v. 18, p. 955–958.

——1999, Hydrothermal processes related to movement of fluid from plastic into brittle rock in the magmatic-epithermal environment: Economic Geology, v. 94, p. 1193–1211.

Gruen, G., Heinrich, C.H., and Schroeder, K., 2010, The Bingham Canyon porphyry Cu-Mo-Au deposit. II. Vein geometry and ore shell formation by pressure-driven rock extension: Economic Geology, v. 105, p. 69–90.

Gustafson, L.B. and Hunt, J.P., 1975, The porphyry copper deposit at El Salvador, Chile: Economic Geology, v. 70, p. 857–912.

Gustafson, L.B., and Quiroga G., J., 1995, Patterns of mineralization and alteration below the porphyry copper orebody at El Salvador, Chile: Economic Geology, v. 90, p. 2–16.

Harris, A.C., Golding, S.D., and White, N.C., 2005, Bajo de la Alumbrera copper-gold deposit: Stable isotope evidence for a porphyry-related hydrothermal system dominated by magmatic aqueous fluids: Economic Geology, v. 100, p. 863–886.

Hedenquist, J.W., and Lowenstern, J.B., 1994, The role of magmas in the formation of hydrothermal ore deposits: Nature, v. 370, p. 519–527.

Heinrich, C.A., Guenther, D., Audetat, A., Ulrich, T., and Frischknecht, R., 1999, Metal fractionation between magmatic brine and vapor, determined by microanalysis of fluid inclusions: Geology, v. 27, p. 755–758.

Heithersay, P.S., and Walshe, J.L., 1995, Endeavor 26 North: A porphyry copper-gold deposits in the Late Ordovician shoshonitic Goonumbla Volcanic Complex, New South Wales, Australia: Economic Geology, v. 90, p. 1506–1532.

Hemley, J.J., and Hunt, J.P., 1992, Hydrothermal ore-forming processes in the light of studies in rock-buffered systems: II. Some general geologic applications: Economic Geology, v. 87, p. 23–43.

Inan, E. and Einaudi, M.T., 2002, Nukundamite ($Cu_{3.38}Fe_{0.62}S_4$)-bearing copper ore in the Bingham Porphyry Deposit, Utah: Result of upflow through quartzite: Economic Geology, v. 97, p. 499–515.

James, A.H., Smith, W.H., and Bray, R.E., 1961, Bingham district; a zoned porphyry ore deposit: Utah Geological Society Guidebook 16, p. 81–100.

James, L.P., 1978, The Bingham copper deposits, Utah, as an exploration target: History and pre-excavation geology; Economic Geology, v. 73, p. 1218–1227.

John, D.A., 1989, Geologic settings, depths of emplacement, and regional distribution of fluid inclusions in intrusions of the central Wasatch Mountains, Utah: Economic Geology, v. 84, p.386–409.

——1998, Geologic setting and characteristics of mineral deposits in the Central Wasatch Mountains, Utah: Society of Economic Geologists, Guidebook Series, v. 29 (2nd edition), p. 11–33.

John, E.C., 1978, Mineral zones in the Utah copper orebody: Economic Geology, v. 73, p. 1250–1259.

Keith, J.D., Whitney, J.A., Hattori, K., Ballantyne, G.H., Christiansen, E.H., Barr, D.L., Cannan, T.M., and Hook, C.J., 1998, The role of magmatic sulfides and mafic alkaline magmas in the Bingham and Tintic mining districts, Utah: Journal of Petrology, v. 38, p. 1679–1690.

Landtwing, M.R., Pettke, T., Halter, W.E., Heinrich, C.A., Redmond, P.B., Einaudi, M.T., and Kunze, K., 2005, Copper deposition during quartz dissolution by cooling magmatic-hydrothermal fluids: The Bingham porphyry: Earth and Planetary Science Letters, v. 235, p. 229–243.

Landtwing, M.R., Furrer, C., Redmond, P. B., Pettke, T., Guillong, M., and Heinrich, C.A., 2010, The Bingham Canyon porphyry Cu-Mo-Au deposit: III. Zoned copper-gold ore deposition by magmatic vapor expansion: Economic Geology, v. 105, p. 91–118.

Lanier, G., John, E.C., Swensen, A.J., Reid, J., Bard, C.E., Caddey, S.W., and Wilson, J.C., 1978a, General geology of Bingham mine, Bingham Canyon, Utah: Economic Geology, v. 73, p. 1228–1241.

Lanier, G., Raab, W.J., Folsom, R.B., Cone, S., Moore, W.J., and Wilson, J.C., 1978b, Alteration of equigranular monzonite, Bingham mining district, Utah: Economic Geology, v. 73, p. 1270–1286.

Lickfold, V., Cooke, D.R., Smith, S.G., and Ullrich, T.D., 2003, Endeavour copper-gold porphyry deposits, Northparkes, New South Wales: Intrusive history and fluid evolution: Economic Geology, v. 98, p. 1607–1636.

Melker, M.D., and Geissman, J.W., 1998, Paleomagnetism of the Oquirrh Mountains and implications for the Cenozoic structural history of the easternmost Great Basin: Society of Economic Geologists, Guidebook Series, v. 29 (2nd edition), p. 101–112.

Meyer, C., 1965, An early potassic type of alteration at Butte, Montana: American Mineralogist, v. 50, p. 1717–1722.

Moore, W.J., 1970, Igneous rocks in Bingham mining district, Utah: Unpublished Ph.D. thesis, Stanford University, 184 p.

Moore, W.J., and Czamanske, G.K., 1973, Compositions of biotites from unaltered and altered monzonitic rocks in the Bingham mining district, Utah: Economic Geology, v. 68, p. 269–274.

Nash, J.T., 1976, Fluid-inclusion petrology; data from porphyry copper deposits and applications to exploration: U.S. Geological Professional Paper, 907 D, p. 1–16.

Parry, W.T., Wilson P.N., Jasumback, M.D., and Heizler, M.T., 1998, Clay mineralogy and $^{40}Ar/^{39}Ar$ dating of phyllic and argillic alteration at Bingham Canyon, Utah: Society of Economic Geologists, Guidebook Series, v. 29 (2nd edition), p. 171–188.

Parry, W.T., Wilson, P.N., Moser, D., and Heizler, M.T., 2001, U-Pb dating of zircon and $^{40}Ar/^{39}Ar$ dating of biotite at Bingham, Utah: Economic Geology, v. 96, p. 1671–1683.

Parry, W.T., Jasumback, Mark, and Wislon, P.M., 2002, Clay mineralogy and phyllic and intermediate argillic alteration at Bingham, Utah: Economic Geology, v. 97, p. 221–239

Perelló, J. Neyra, C., Posso, H., Zárate, A., Ramos, P., Caballero, A., Martini, R., Fuster, N., and Muhr, R., 2004, Cotabambas: Late Eocene porphyry copper-gold mineralization southwest of Cuzco, Peru: Society of Economic Geologists Special Publication, v. 11, p. 213–230.

Phillips, C.H., Smith, T.W., and Harrison, E.D., 1998, Alteration, metal zoning, and ore controls in the Bingham Canyon porphyry copper deposit, Utah: Society of Economic Geologists, Guidebook Series, v. 29 (2nd edition), p. 133–145.

Presnell, R.D., 1998, Structural controls on the plutonism and metallogeny in the Wasatch and Oquirrh Mountains, Utah: Society of Economic Geologists, Guidebook Series, v. 29 (2nd edition), p. 1–9.

Proffett, J.M., 2003, Geology of the Bajo de la Alumbrera porphyry copper-gold deposit, Argentina. Economic Geology, v. 98, p. 1535–1574.

——2009, High Cu grades in porphyry Cu deposits and their relationship to emplacement depth of magmatic sources: Geology, v. 37, p. 675–678.

Redmond, P.B., 2002, Magmatic-hydrothermal fluids and copper-gold ore formation at Bingham Canyon, Utha: Unpublished Ph.D. thesis, Stanford University, 228 p.

Redmond, P.B., Einaudi, M.T., Inan, E.E., Landtwing, M.R., Heinrich, C.A., 2004, Copper deposition by fluid cooling in intrusion-centered systems: New insights from the Bingham porphyry ore deposit, Utah: Geology, v. 32, p. 217–220.

Reyes, A.G., 1990, Petrology of Philippine geothermal systems and the application of alteration mineralogy to their assessment: Journal of Volcanology and Geothermal Research, v. 43, p. 279–309.

Reynolds, T.J., and Beane, R.E., 1985, Evolution of hydrothermal fluid characteristics at the Santa Rita, New Mexico, porphyry copper deposit: Economic Geology, v. 80, p. 1328–1347.

Roedder, E., 1971, Fluid inclusion studies on the porphyry-type ore deposits at Bingham, Utah, Butte, Montana, and Climax, Colorado: Economic Geology, v. 66, p. 98–118.

Roberts, R.J., Crittenden, M.D.J., Tooker, E.W., Morris, H.T., Hose, R.K., and Cheney, T.M., 1965, Pennsylvanian and Permian basins in northwestern Utah, northeastern Nevada, and south-central Idaho: American Association of Petroleum Geologists Bulletin, v. 49, p. 1926–1956.

Roberts, S.A., 1973, Pervasive early alteration in the Butte district, Montana, in Miller, R.N. ed., A Field Meeting held August 18–21, 1973, Butte, Montana: Society of Economic Geologists, U.S. Geological Survey, and Anaconda Company, Geological Department, p. HH1–HH8.

——1975, Early hydrothermal alteration and mineralization in the Butte district, Montana: Unpublished Ph.D. dissertation, Cambridge, Mass., Harvard University, 157 p.

Roedder, E., 1971, Fluid incluson studies on the porphyry type ore deposits at Bingham, Utah, Butte, Montana, and Climax, Colorado: ECONOMIC GEOLOGY, v. 66, p. 98–120.

Rubright, R.D., and Hart, O.J., 1968, Non-porphyry ores of the Bingham district, Utah, *in* Ridge, J.D., ed., Ore Deposits of the United States, 1933–1967: American Institute of Mining, Metallurgical, and Petroleum Engineers, p. 886–907.

Rusk, B.G., 2003, Cathodoluminescent quartz textures and fluid inclusions in veins of the porphyry copper-molybdenum deposit in Butte, Montana: Constraints on the physical and chemical evolution of the hydrothermal system, Unpublished Ph.D. dissertation, Eugene, Oregon, University of Oregon, 285 p.

Rusk, B.G, Reed, M.H, and Dilles, J.H., 2008, Fluid inclusion evidence for magmatic-hydrothermal fluid evolution in the porphyry copper-molybdenum deposit at Butte, Montana: ECONOMIC GEOLOGY, v. 103, p. 307–334.

Seedorff, E., and Einaudi, M.T., 2004, Henderson porphyry molybdenum system, Colorado: I. Sequence and abundance of hydrothermal mineral assemblages, flow paths of evolving fluids, and evolutionary style: ECONOMIC GEOLOGY, v. 99, p. 3–37.

Sheppard, S.M.F., Nielsen, R L., and Taylor, H.P.J., 1969, Oxygen and hydrogen isotope ratios of clay minerals from porphyry copper deposits: ECONOMIC GEOLOGY, v. 64, p. 755–777.

——1971, Hydrogen and oxygen isotope ratios in minerals from porphyry copper deposits: ECONOMIC GEOLOGY, v. 66, p. 515–542.

Smith, W.H., 1975, General structural geology of the Bingham mining district, *in* Bray, R.E., and Wilson, J.C., eds., Guidebook to Bingham mining district: Society of Economic Geologists, p. 41–48.

Stewart, J.H., Moore, W.J., and Zietz, I., 1977, East-west patterns of Cenozoic igneous rocks, aeromagnetic anomalies, and mineral deposits, Nevada and Utah: Geological Society of America Bulletin, v. 88, p. 945–991.

Stringham, B.F., 1953, Granitization and hydrothermal alteration, at Bingham, Utah: Geological Society of America Bulletin, v. 64, p. 945–991.

Tooker, E.W., 1971, Regional structure controls of ore deposits, Bingham mining district, Utah, U.S.A.: Geological Society of Japan, Special Issue 3, p. 76–81.

Tosdal, R.M., and Richards, J.P., 2001, Magmatic and structural controls on the development of porphyry Cu±Mo±Au deposits: Reviews in Economic Geology, v. 14, p. 157–181.

Ulrich, T., Guenther, D., and Heinrich, C.A., 1999, Gold concentrations of magmatic brines and the metal budget of porphyry copper deposits: Nature, v. 399, p. 676–679.

——2002, The evolution of a porphyry Cu-Au deposit, based on LA-ICP-MS analysis of fluid inclusions: Bajo de la Alumbrera, Argentina: ECONOMIC GEOLOGY, v. 97, p. 1889–1920.

Vogel, T., Cambray, F. N., Feher, L., Constenius, K., and Team, W.R., 1997, Petrochemistry and emplacement history of the Wasatch igneous belt: Society of Economic Geologists, Guidebook Series, v. 29 (2nd edition), p. 35–46.

Waite, K.A., Keith, J.D., Christiansen, E.H., Whitney, J.A., Hattori, K., Tinagey, D.G., and Hook, C. ., 1998, Petrogenesis of the volcanic and intrusive rocks associated with the Bingham Canyon Porphyry Cu-Au-Mo deposit, Utah: Society of Economic Geologists, Guidebook Series, v. 29 (2nd edition), p. 69–90.

Wilson, J C., 1978, Ore fluid-magma relationships in a vesicular quartz latite porphyry dike at Bingham, Utah: ECONOMIC GEOLOGY, v. 73.

Welsh, J.E., and James, A.H., 1961, Pennsylvanian and Permian stratigraphy of the central Oquirrh Mountains, *in* Cook, D.R., ed., Geology of the Bingham mining district and northern Oquirrh Mountains: Utah Geological Society, Guidebook to the Geology of Utah, no. 16, p. 1–16.

Zietz, I., Bateman, P.C., Case, J.E., Crittenden, M.D.J., Griscom, A., King, E.R., Roberts, R.J., and Lorentzen, G.R., 1969, Aeromagnetic investigation of crustal structure for a strip across the western United States: Geological Society of America Bulletin, v. 80, p. 1703–1714.

APPENDIX 1

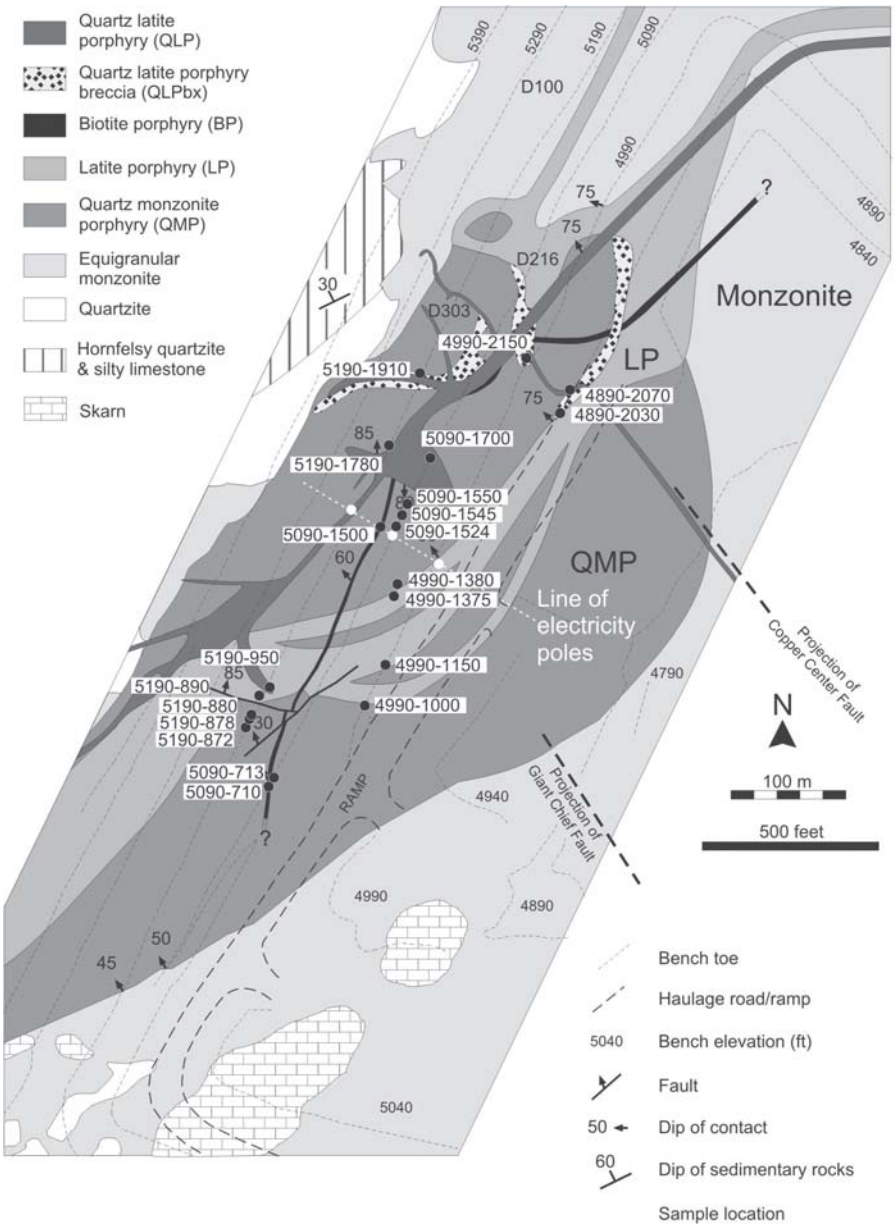

FIG. A1. Geology map (the same as Fig. 3) showing the location of samples mentioned in the text and figure captions.

TABLE A1. Chip Sample Assay Data

	Assay no.	Sample no.	Rock type	Cu (%)	Au (ppm)	Ag (ppm)	Mo (ppm)
1	98008	5090 - 1500	BP	3.50	7.14	25.40	696
2	98009	5090 - 1545	QMP	1.50	2.63	10.50	68
3	98022	5190 - 872	QMP	2.00	5.17	17.10	577
4	98023	5190 - 872	QMP	2.30	7.31	20.60	794
5	98024	5190 - 878	QMP	1.20	3.82	10.60	369
6	98025	5190 - 880	QMP	2.10	6.29	19.40	118
7	98026	5190 - 890	LP	0.58	1.37	3.40	809
8	98027	5190 - 890	LP	0.37	0.67	2.40	213
9	98028	5190 - 950	QLP	0.13	0.10	<0.2	35
10	98029	5090 - 1700	QLP	1.90	4.48	15.10	182
11	98033	5190 - 1910A	QMP	2.20	5.66	20.20	324
12	98034	5190 - 1910B	QLPBx	0.21	0.37	1.10	41
13	98041	4990 - 1375	LP	0.67	0.83	3.60	227
14	98044	4990 - 1380	QMP	2.50	5.77	19.80	270
15	98052	4890 - 2070	QLP	0.08	0.05	<0.2	5
16	99003	5090 - 710	BP	1.45	3.02	10.20	546
17	99004	5090 - 713	QMP	0.57	1.67	3.60	213
18	99026	5090 - 1524	QMP	2.90	10.04	23.10	155

Notes: Assays by Intertek Testing Services (Bondar Clegg Inc.); copper, silver, and molybdenum were analyzed by standard multi-acid (HF-HNO_3-$HClO_4$-HCl) digestion followed by induced coupled plasma (ICP) analysis; gold analysis was carried out by standard fire assay–AA technique; sample size varied from 0.5 to 6 kg; all sample numbers above prefixed with either 4890-, 4990-, 5090-, or 5190- were collected in the open pit by Redmond during the summer of 1998 and 1999; these numbers refer to the bench elevation (in ft) on which they were collected (see Fig. 4); the second part of the sample no. refers to the horizontal distance in feet from a reference point on each bench; the reference point on each bench was an electricity pole arbitrarily designated as 1,500 feet (increasing to the northeast along each bench); this line of poles is shown on the location map above; for example, sample 5090-1524 was collected 24 feet to the northeast of the pole on bench 5090

APPENDIX 2

TABLE A2. Whole-Rock XRF Analyses of BP

Whole-rock analyses

Assay no.	Biotitized BP[1] 99001	Biotitized BP[1] 99006	Biotitized BP 98008	Biotitized BP 99003	Minette dike[2] Bing-38	Minette flow[3] Tick 43
Sample no.	5090-696	4890-pipe9	5090-1500	5090-710		
SiO_2	60.90	62.02	59.30	61.76	57.93	44.21
TiO_2	0.56	0.55	0.49	0.55	0.67	0.89
Al_2O_3	12.70	12.72	12.19	12.09	12.98	10.31
Fe_2O_3	2.80	3.46	4.25	3.25	10.85	11.42
MnO	0.01	0.02	0.01	0.02	0.04	0.20
MgO	9.49	8.06	7.25	8.87	8.67	15.00
CaO	0.67	0.72	0.63	0.65	1.11	10.65
Na_2O	0.20	0.34	0.42	0.21	1.17	3.87
K_2O	10.46	9.42	9.72	9.64	5.89	3.07
P_2O_5	0.41	0.38	0.38	0.36	0.71	0.38
S	0.41	0.52	1.19	0.57	0.41	0
F	0.88	0.64	0.63	0.75	0.36	0.34
Cl	0.01	0.01	0.01	0.01	0.10	0.01
Cu	0.86	1.10	2.7	1.28	0.32	0.01
Total	100.38	99.95	99.17	100.01	101.21	100.36
LOI	NA[4]	NA[4]	NA[4]	NA[4]	3.6	2.06
Sc (ppm)	14	24	9	18	16	22
V	156	126	116	129	159	148
Cr	350	351	279	366	353	1201
Ni	140	124	124	140	472	349
Ga	23	19	19	20	17	14
As	9	3	2	8	NA	NA
Rb	283	256	223	257	342	85
Sr	99	122	84	112	46	752
Y	13	10	7	10	13	24
Zr	139	133	111	123	184	121
Nb	11	7	2	6	14	23
Mo	273	356	427	437	NA	NA
Ba	1683	1222	1011	1606	809	1700
La	64	47	42	48	46	69
Ce	128	91	91	90	111	84
Nd	47	37	38	37	47	47
Sm	8	7	6	7	9	10
Pb	11	13	14	16	5	13
Th	26	30	32	31	29	4
U	6	6	5	5	8	2

[1] Samples analyzed by David Tingey Analytical Consulting (DTAC), Springville, Utah, on 2 gram pressed powder pellets backed with cellulose; elemental analyses by wave-length dispersive XRF (Bruker (Siemens) SRS 303) calibrated with international reference standards; see Appendix 1, Fig. A1, for sample locations

[2] Bing-38 analysis courtesy of Jeffrey Keith, Brigham Young University; description of Bing-38 can be found in Deino and Keith (1998)

[3] Waite et al. (1998)

[4] LOI not determined, sulfur volatilization prevents accurate measurement